DYNAMIC ADAPTABLE ANTENNA ARRAYS FOR WIRELESS COMMUNICATION NETWORKS

A THESIS SUBMITTED TO THE GRADUATE DIVISION OF THE UNIVERSITY OF HAWAI'I IN PARTIAL FULFILLMENT OF THE REQUIREMENTS FOR THE DEGREE OF

MASTER OF SCIENCE

IN

ELECTRICAL ENGINEERING

AUGUST 2006

By
Justin Roque

Thesis Committee:

Wayne A. Shiroma, Chairperson
Tep Dobry
Eric L. Miller

We certify that we have read this thesis and that, in our opinion, it is satisfactory in scope and quality as a thesis for the degree of Master of Science in Electrical Engineering.

THESIS COMMITTEE

Chairperson

I dedicate this thesis to my family.

To my Mom, Dad, Brother, and Lauren who have supported me with unconditional love and support throughout the long college road that I have taken.

ACKNOWLEDGEMENTS

First of all I would like to acknowledge Dr. Wayne Shiroma for giving me the opportunity to join his research group and further my education. The interesting work, conferences, and papers we have published would have not been possible without the commitment and enthusiasm that he has shared with all of his students.

Next I would like to thank the committee members Dr. Dobry and Dr. Miller. Dr. Dobry for his guidance through my undergraduate studies and whose EE260 class has kept me motivated to stick with electrical engineering. Dr. Miller for his passion for engineering will continue to influence many more undergraduate and graduate electrical engineers in their academic careers.

I would like to thank my fellow researchers. I have had the opportunity to work with "two sets" of MMRL groups. The first being the era of Dr. Ryan Miyamoto, I have learned a lot from his guidance and would like to thank him for his patience and teaching. To the members of the MMRL group during this period, Kendall Ching, Blaine Murakami, Stephen Sung, Joe Cardenas, TJ Mizuno, and Cheyan Song I would like to thank you for all the support and encouragement that has allowed me to get this far. A thank you to the present members of the MMRL group, Brandon Takase, Ryan Pang, Justin Akagi, and Monte Watanabe whom I know will carry research to the next level. A special thanks to Grant Shiroma who has taken the role of mentor to the present members of the MMRL group and has always helped me when I was in a bind.

Lastly, I would like to thank the sponsors for all the research done in this thesis. Funding was provided by the following sponsors AFRL, NASA, AFOSR, AIAA, NGST, and Oceanit Laboratories.

ABSTRACT

Many wireless systems are being incorporated into a single device. Combining different wireless systems in one package simplifies circuitry, increases efficiency and allows users to use one interface to access many systems. Phased arrays and retrodirective arrays improve the performance at the antenna front end. Reconfigurable networks eliminate redundant circuitry in the wireless subsystems and allow sharing of specific components.

This thesis presents advances in satellite-to-satellite communication systems, mobile terrestrial to satellite systems, and a method of characterizing a class of reconfigurable circuits. First, a two-dimensional retrodirective array using quadruple subharmonic mixing is designed at 10.5 GHz for satellite-to-satellite communication. Two small satellites demonstrated a retrodirective link with tracking ranging from -40° to 40°. Secondly, a two-dimensional transmit frequency-controlled phased array is presented. Simple voltage controlled steering of the phased array makes for easy integration with external tracking and control systems. A scanning range of 40° per axis has been demonstrated. Lastly a method for characterizing a reconfigurable MEMS tunable matching network has been presented and verified by circuit simulation. As more systems require communication at different frequencies, variable-frequency components require using tunable matching networks. Characterization of the matching networks becomes an issue when troubleshooting modules within wireless communication devices.

TABLE OF CONTENTS

LIST OF TABLES

LIST OF FIGURES

CHAPTER 1

INTRODUCTION

A large number of today's communication systems consist of groups of smaller subsystems linked together in one form or another. The most common example of this is a cellular phone communication system. Cellular phones have made it possible to communicate with people on the other side of the globe. Following the path of the cellular phone signal, up to three types of wireless communication systems are used. The first is the connection of the mobile transponder to the local service provider tower. Second, the tower is linked to a mainframe and the signal is transmitted to orbiting satellites. Lastly, the satellite may have to relay the signal to another orbiting satellite and have the signal transmitted back to a ground station on the other side of the world. In this example, three wireless paths are evident, a mobile terrestrial to fixed terrestrial system, a terrestrial to satellite system, and a satellite-to-satellite system.

Companies such as DirectTV and Wildblue are investing $1.4 billion into the latest communication satellites, SPACEWAY 1 & 2 [1], [2]. The SPACEWAY broadband satellite network hopes to provide not only voice communication, but high-speed communications for internet, data, video, and multimedia applications [3]. Another example of combining multiple wireless communication systems and applications is the military's Mobile Modular Command Center (M2C2), Fig. 1.6 [4]. Hawaii technology companies are combining efforts to outfit a Humvee with radio and

satellite communication equipment capable of providing video, teleconferencing, and secure data transmission.

Fig. 1.1: Picture of the Mobile Modular Command Center (M2C2)

Combining different wireless systems reduces circuitry, reduces cost, improves efficiency, and increases overall performance. This thesis focuses on improving wireless communication systems by building on a basic system, Fig. 1.2 (a). More specifically, this thesis introduces antenna arrays that improve satellite-to-satellite communications and mobile to satellite communications (Fig. 1.2(b)), and finally, combining many wireless systems (Fig. 1.2(c)) is modified with reconfigurable adaptive circuitry to reduce circuitry in combined systems (Fig. 1.2(d)).

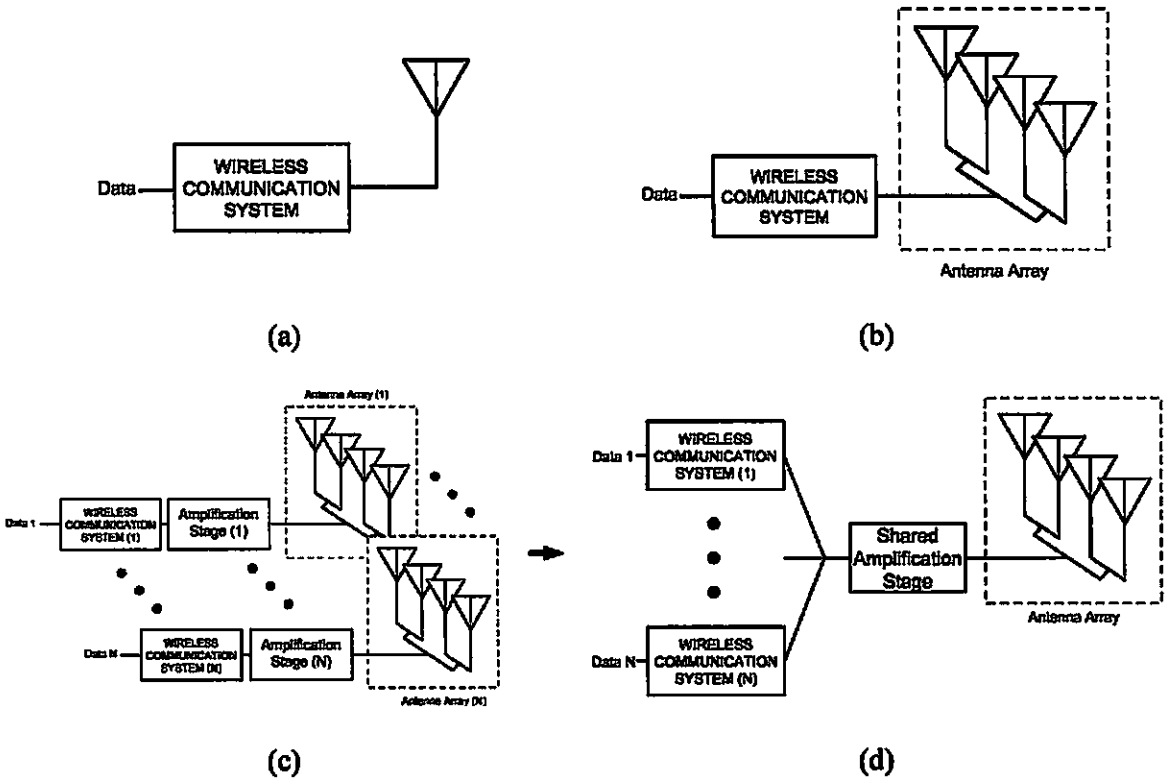

Fig. 1.2: (a) Basic wireless communication system with single omnidirectional antenna, (b) Antenna array circuitry added to basic wireless system, (c) N wireless communication systems, (d) N wireless communication systems sharing amplification stage and antenna array

1.1 Omnidirectional Antennas

Omnidirectional antennas are the simplest and most common means for broadcasting electromagnetic waves into free space. Fig. 1.3 depicts an omnidirectional antenna and its propagation characteristics. Single-wire construction makes this type of antenna cost effective. The electromagnetic signals radiate in all directions allowing users to communicate with one another without knowing the positions of other user antennas.

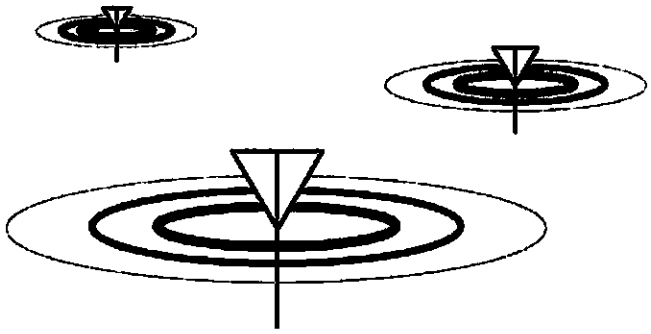

Fig. 1.3: Omnidirectional antenna radiating power in all directions

An omnidirectional antenna may be a cost-effective solution for commercial applications. However, there are downsides associated with broad radiation patterns. In transmission, power is radiated inefficiently in all directions. The signal can possibly interfere with other systems and is susceptible to eavesdropping. In reception, signals in all directions including interference and jamming signals are received. These characteristics cause vulnerabilities in a security-sensitive communication system.

1.2 Phased Arrays

The efficiency and security of a wireless system is greatly increased if the power transmitted by an antenna is focused only on the target. The easiest method of focusing electromagnetic power is manipulating the phases of antenna arrays. Typical phased arrays produce focused beams significantly reducing receive and transmit interference and allows controllable electronic steering.

A. *Conventional Phased Array Methods*

Phased arrays are the simplest method of beam forming. In Fig. 1.4 each antenna element is connected to a phase shifter. To steer the beam the phase shifters delay the signal and a phase progression from element to element will steer the beam. The downside of the conventional phased array is the expensive phase shifters this method requires. In large arrays, the phase shifter control circuitry can become complex.

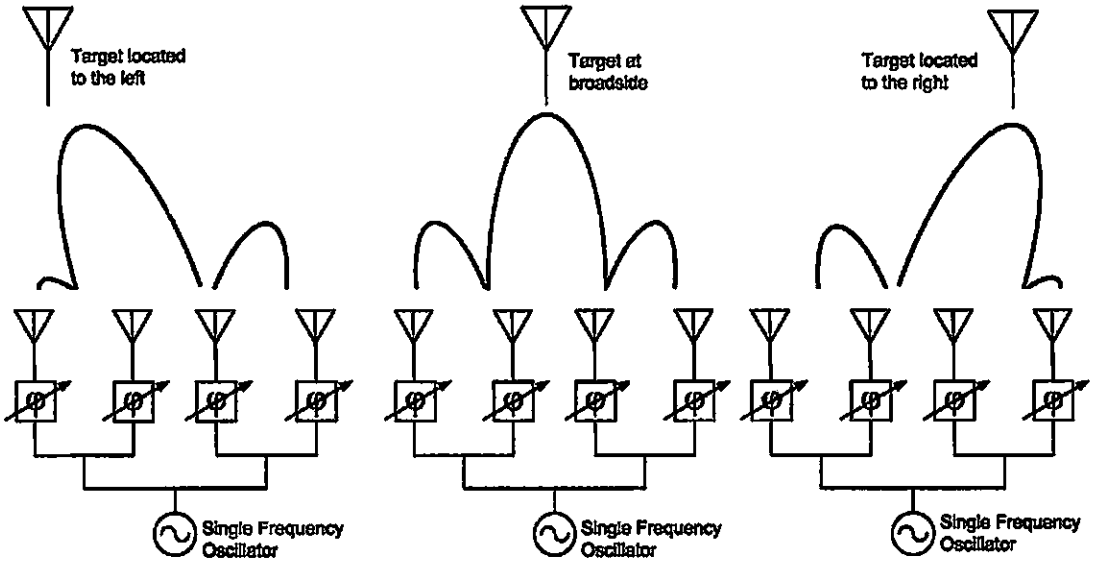

Fig. 1.4: Conventional array using phase shifters

B. *Frequency-Scanned Phased Arrays*

One of the drawbacks in conventional phased-array antenna systems, especially large ones, is the cost and complexity associated with individual phase shifters at each radiating element. An alternative method of beam steering that requires no phase shifter components, other than fixed delay lines between radiating elements, is the frequency-

scanned array [5]. Progressively phased delay lines feed antenna elements. The linear relationship between frequency and phase in the feed network causes varying phase progression when tuning the output frequency (Fig. 1.5).

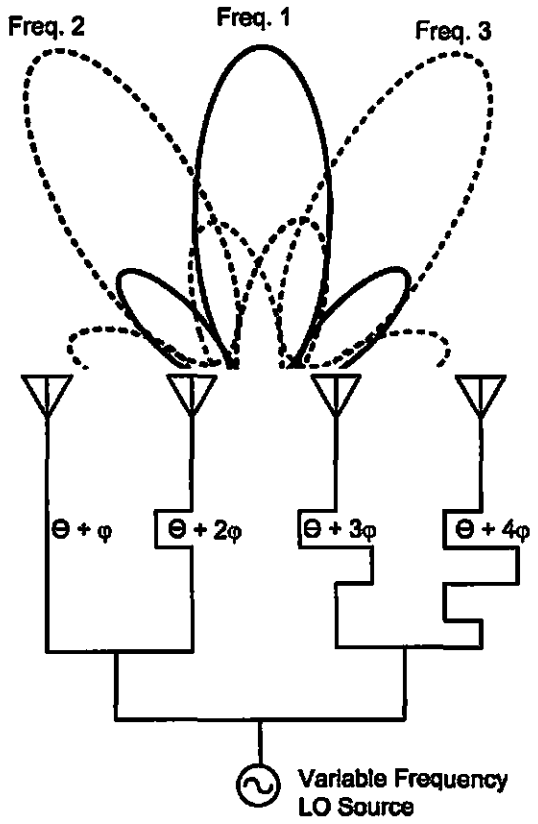

Fig. 1.5: Figure of frequency scanned array

C. *Frequency-Controlled Phased Arrays*

The frequency scanned array is well suited for radar applications, but most communication systems require a constant transmission frequency. For systems requiring a fixed radiating frequency, heterodyne mixers can be inserted at each element

[5], [6]. Fig. 1.6 shows the basic layout of this system. The radio frequency (RF) signal appearing at each antenna element is a result of mixing an intermediate frequency (IF) signal and a local oscillator (LO) signal, both of which are fed to each mixer via feed networks. A set of delay lines is incorporated into the LO feed network, so that the LO voltage-controlled oscillator controls the beam direction, as in a standard frequency-scanned array. As the LO VCO frequency varies, the IF frequency must also be varied, such that the difference between these frequencies, i.e. the RF frequency, remains the same.

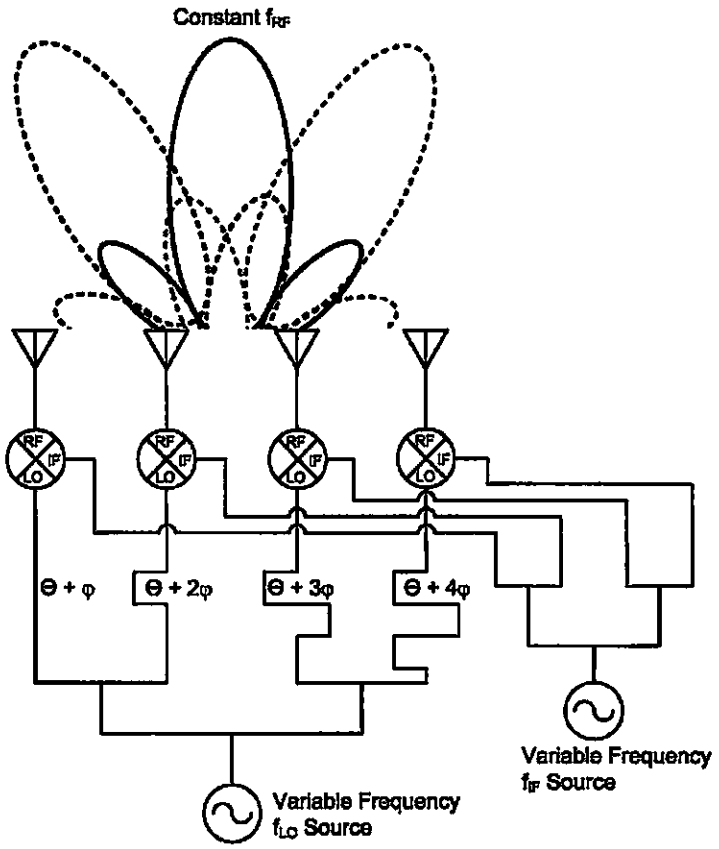

Fig. 1.6: General heterodyne-scan phased-array architecture used in [7]-[10]. Two VCOs are required to maintain a constant RF.

1.3 Retrodirective Arrays

A major disadvantage of phased arrays is that the user must know where to steer the beam before transmission. A preferred solution is one in which signals can be transmitted automatically in the same direction as the received signals, a quality retrodirective arrays provide. On top of self-tracking, both efficiency and security are increased with negligible increase in circuit complexity.

A. Corner Reflector

The corner reflector [11] is the simplest retrodirective device. Fig. 1.7 depicts the corner reflector consisting of two perpendicular metal plates. An incoming signal is reflected back to the direction it originated. Though corner reflectors produce retrodirectivity, applications are limited to radar targets and markers. Implementing and integrating circuitry into corner reflectors is quite difficult.

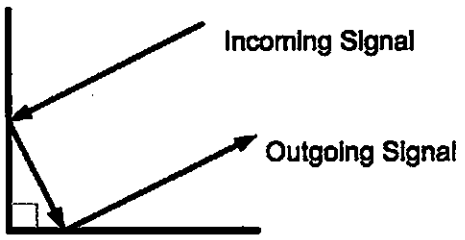

Fig. 1.7: Corner Reflector

B. Van Atta Array

The Van Atta array (Fig. 1.8) is another method of implementing retrodirectivity [12]. The array uses pairs of antenna elements that are spaced equidistant from the center

of the array. As the incoming wave crosses the array, a phase progression occurs. As the signal propagates through the transmission lines, the outgoing wave across the array has a phase progression opposite of the incoming wave. The opposite phase progression means the outgoing wave propagates back in the same direction of the incoming wave.

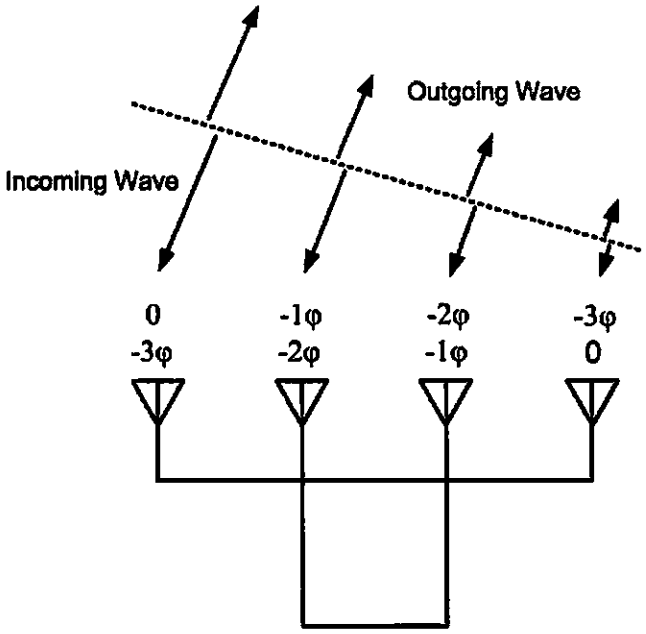

Fig. 1.8: Schematic of Van Atta Array

Like the corner reflector, the Van Atta array demonstrates retrodirectivity. However, to achieve highly directive beams, more elements are required. As the number of elements increase in a Van Atta array, the design becomes considerably more difficult due to routing the transmission lines between each pair of elements.

C. Phase-Conjugating Array

Phase conjugation is the third method applied to retrodirective arrays [13]. Fig. 1.9 depicts a phase-conjugating array in which an incoming wave causes a phase

progression across the array. If each element uses a phase conjugator at each element, the resultant outgoing wave will have a phase progression opposite of the original incoming wave. Like the Van Atta array, the outgoing wave is in the same direction as the incoming wave.

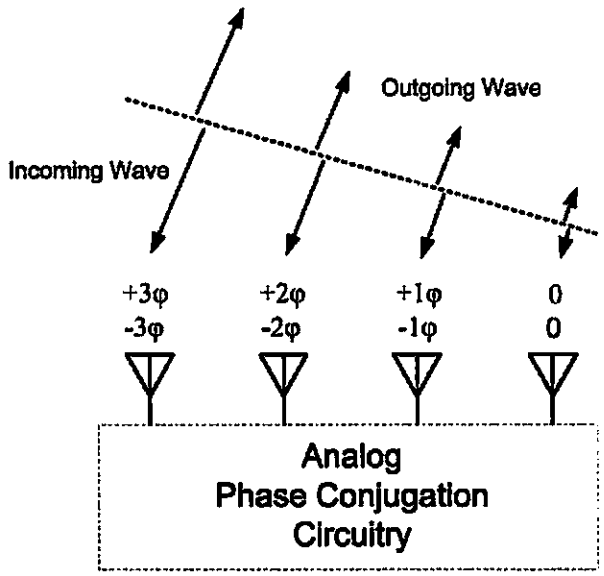

Fig. 1.9: Phase conjugating array

1.4 Retrodirective Arrays for Small-Satellite Networks

Typical communication satellites cost developers hundreds of millions of dollars, have long lead times, are expensive to launch, and can be prone to single-point failures. Alternatives to large satellites are the use of small satellites configured in a network. Small satellites in the past 20 years have shown their potential for their low-profile and low-cost characteristics [14]. The military, commercial, academic and research fields have shown interest in the operation, fabrication, and development of such systems.

Small satellites have gained popularity for short-term missions. Experimental payloads such as sensor testing, communication demonstrations and imaging are a few experiments being proposed for small-satellite research. These networks also promise increased mission flexibility by distributing mission task amongst the network. These networks also reduce the chances of single-point failures. If a node in the network fails, its tasks can be re-distributed to the other nodes. One of the greatest challenges, especially in a reconfigurable one, is the communication aspect in which each node must establish and maintain communications without prior knowledge of each other's location.

One class of small-satellites has dimensions of a 10 x 10 x 10 cm cube. Conventional propulsion systems are too large to be mounted into small satellites, making communication between satellites challenging. Self-steering arrays increase communication efficiency in addition to increasing security. Chapter 2 discusses a small satellite outfitted with a retrodirective array.

1.5 Mobile Communication Arrays

The M2C2 project currently uses a mechanically driven satellite dish mounted on top of the Humvee, Fig. 1.10. The mechanically driven nature of the satellite dish may be too slow for the vehicle's constant movement. The large dome also makes the vehicle conspicuous to enemy forces. Electronically steered phased arrays can provide fast tracking capabilities than their mechanically driven counterparts. The phased array circuitry is concealed in the Humvee and only the antenna array is externally mounted.

Fig. 1.10: Picture of M2C2 with external satellite dish

1.6 Reconfigurable Networks

The M2C2 project mentioned earlier combines many communication systems, all operating at different frequencies. To reduce circuitry size specific parts of an RF system can be combined. One specific example is the transmit amplifier at the antenna. To ensure signal amplitudes are high enough for recoverability the RF signals are amplified. Amplifiers are the most common method to increase the power of a signal. In most cases, the amplifier is designed to amplify a specific frequency band. But with modern technologies merging together a wide frequency spectrum is often preferred. This is especially true for military applications. Currently separate wireless systems are used such as a SATCOM system operating at 14.4-15.35 GHz, an enhanced position location reporting system at 420-450 MHz, cell phone relay capabilities at 1.9 GHz, a secure wireless LAN at 2.4 GHz, and a GPS tracking system at 1.2 GHz and 1.5 GHz.

One solution is the use of reconfigurable amplifiers that can be adapted and tuned to meet the power requirements on any frequency allocation band. This could mean

melding all communication equipment so soldiers in the field can have a versatile and robust communication system.

The latest reconfigurable networks use Micro-Electro-Mechanical Systems (MEMS). These devices usually consist of many switches that can change the impedance of the transmission lines connected to the amplifier (Fig. 1.11) [15]. The amplifier can be tuned for a specific frequency and/or amplitude output.

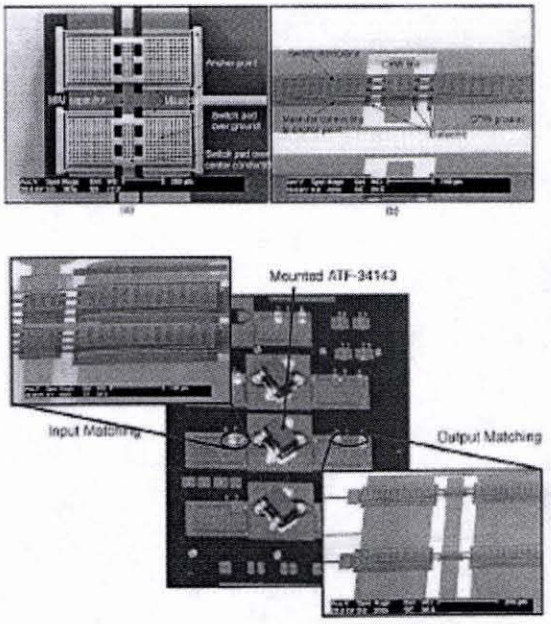

Fig. 1.11: Photographs of MEMS switches in matching networks [15]

One of the difficulties of using MEMS matching networks is accounting for fabrication imperfections once the network is embedded into the communication system. Chapter 4 discusses methods to characterize the matching networks used in such schemes.

1.7 Organization of Thesis

Chapter 2 discusses the application of retrodirective arrays in secure small satellite networks. The quadruple subharmonic mixing technique has allowed array design to account for the limited space and DC power of the satellite.

An electronically steered phased array is discussed in Chapter 3 as an alternative to a mechanically steered satellite tracking dish for mobile applications. A one-dimensional full-duplex and two-dimensional transmit frequency-controlled phased array is designed and demonstrated. Simple steering control is emphasized to avoid complexities and ease integration with tracking and control systems.

Chapters 2 and 3 discussed work with the communication antenna arrays. Reducing circuitry is important when combining communication systems. With advances in configurable networks, circuits such as amplifiers and mixers use adaptable adjustable networks to adjust power levels within the system. Chapter 4 introduces methods to characterize such a system and its components.

Lastly conclusions are made. Further ideas and thoughts for future research are discussed in Chapter 5.

CHAPTER 2

RETRODIRECTIVE ANTENNA ARRAYS FOR USE IN SMALL SATELLITE NETWORKS[1]

2.1 Introduction

From 2003 to 2005 the University of Hawaii engineered the Hokulua (Twin Stars) project. The University of Hawaii received a $100,000 grant funded by the Air Force Office of Scientific Research (AFOSR), and mentored by Air Force Research Lab (AFRL), NASA, and the American Institute of Aerospace and Aeronautics (AIAA) [19-21]. The University of Hawaii was one of 13 Universities within the United States participating in a competitive initiative to help develop, fabricate, and launch advanced nanosatellite systems.

Hokulua's mission was to demonstrate and test the applicability of retrodirective array technology for satellite-to-satellite communications within distributed small-satellite networks by designing, fabricating and testing a retrodirective link in a pair of satellites [22]. One satellite houses the retrodirective array and the other is designed as a transponder satellite to validate the retrodirective implementation.

2.2 Design Parameters

To validate a successful mission, the quality of the transmission link between the two orbiting nanosatellites must be analyzed. The power measurements of a transmitted

[1] Portions of this chapter have been published in [16], [17], [18]

and retroreflected continuous wave signal are recorded over a period of time. The free-floating nature of the satellites allows both communication arrays on the satellites to deviate from broadside. A semi-flexible tether is used to prevent the satellites from drifting too far away from each other, while still allowing the satellites a limited range of motion acceptable to test the steering capabilities of the retrodirective array.

One satellite, designated as the transponder, interrogates the retrodirective satellite and receives and measures the power of the retroreflected signal. The other contains the retrodirective array (Fig. 2.1 and Fig. 2.2).

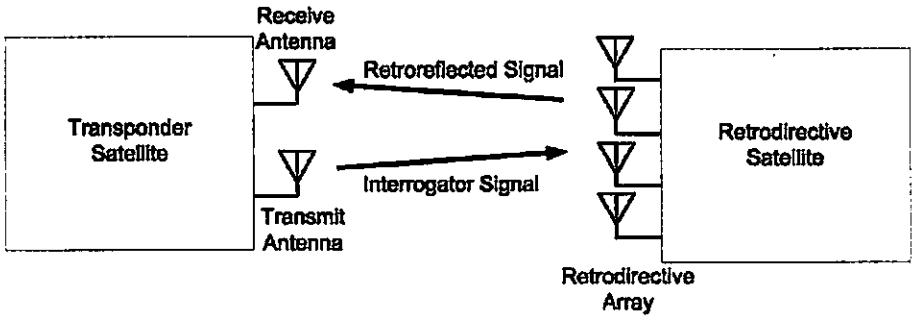

Fig. 2.1: Schematic of satellite communication link

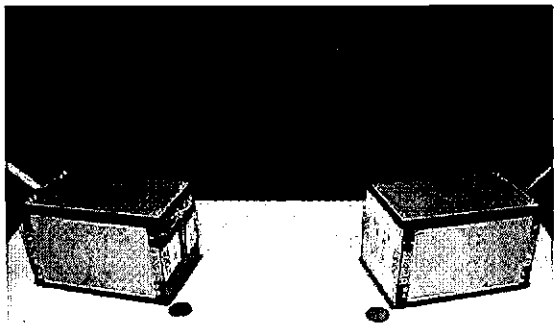

Fig. 2.2: Pair of experimental nanosatellites, retrodirective satellite on the right and interrogator/ receive satellite on the left

The communication system design is influenced by the physical characteristics of the small satellite. First, the free-floating nature of the small satellites makes it necessary to demonstrate a two-dimensional retrodirective array. Secondly, the lack of attitude control requires circularly polarized antennas to prevent polarization mismatches due to varying orientations of the transponder and retrodirective satellite. The designated frequency for the satellite-to-satellite communication system is 10.5 GHz.

Chapter 1 introduced three methods for achieving retrodirectivity. The phase conjugation technique is flexible in design, allowing circuitry to fit within the 10 x 10 x 15 cm satellite housing. The phase conjugation circuitry typically uses heterodyne mixers to achieve phase conjugation, Fig. 2.3 [13]. The next section discusses heterodyne mixing and other phase conjugation methods, analyzed in further detail.

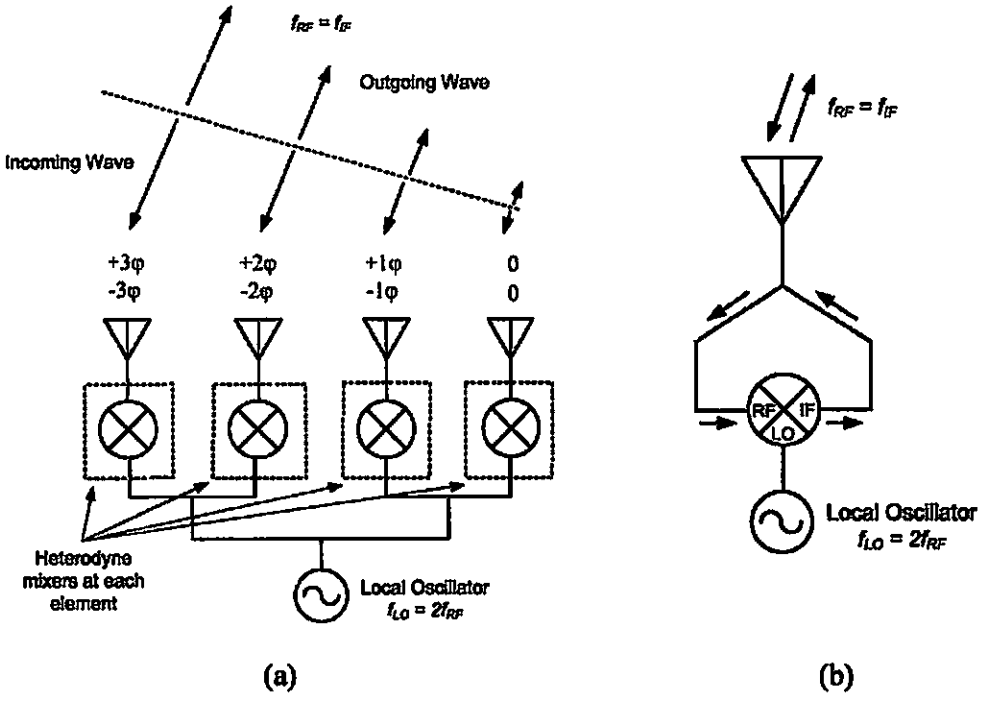

Fig. 2.3: (a) Phase conjugating array using heterodyne mixers at each element, (b) Individual heterodyne mixer and antenna element

2.3 Mixing Techniques

The methods for achieving phase-conjugation are evaluated for the feasibility in our proposed nanosatellite communication system. Due to the volume, power, and budget limitations of the small satellite, different mixing techniques are evaluated, each having their own pros and cons.

A. Fundamental Mixing Technique[2]

Analyzing nonlinear circuits and their associated I/V curves is the traditional way to describe the generation of frequencies. By applying the heterodyne mixing components with non-linear circuit analysis in Fig. 2.4, the associated I/V curve and exponential I/V characteristics can be expressed as a power series [23]:

$$I = aV + bV^2 + cV^3 + dV^4 + eV^5 \ldots \tag{2.1}$$

where *a, b, c, d,* and *e* are constant power series coefficients, unique to specific devices.

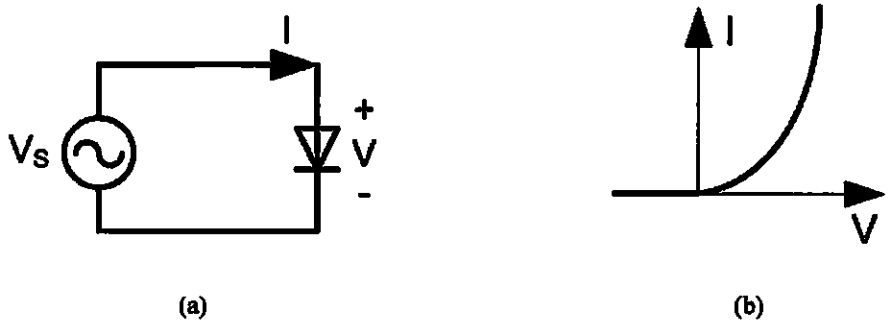

(a) (b)

Fig. 2.4: (a) Diode mixing circuit fed by voltage source, (b) I/V characteristic of diode

If V_s is the sum of both LO and RF signals,

$$V_s = V_1 \cos(\omega_{LO} t) + V_2 \cos(\omega_{RF} t + \varphi) \tag{2.2}$$

[2] This section is reprinted in part from [24] with permission from the author.

If (2.2) is substituted back into (2.1) the first term results in

$$I_a = aV_1\cos(\omega_{LO}t) + aV_2\cos(\omega_{RF}t + \varphi) \tag{2.3}$$

After simplifying through trigonometric identities the second term becomes

$$I_b = \frac{b}{2}\left\{\begin{matrix} V_1^2 + V_2^2 + V_1^2\cos(2\omega_{LO}t) + V_2^2\cos(2\omega_{RF}t + 2\varphi) \\ +2V_1V_2\left[\cos\left((\omega_{LO} + \omega_{RF})t + \varphi\right) + \cos\left((\omega_{LO} - \omega_{RF})t - \varphi\right)\right] \end{matrix}\right\} \tag{2.4}$$

If the LO frequency is set to twice the RF frequency, $\omega_{LO} = 2\omega_{RF}$ and substituted into (2.3) and (2.4), the sum becomes

$$I_a + I_b = \frac{b}{2}\left(V_1^2 + V_2^2\right) + aV_2\cos(\omega_{RF}t + \varphi) + bV_1V_2\cos(\omega_{RF}t - \varphi) \tag{2.5}$$

$$+ aV_1\cos(2\omega_{RF}t) + \frac{bV_2^2}{2}\cos(2\omega_{RF}t + 2\varphi)$$

$$+ bV_1V_2\cos(3\omega_{RF}t + \varphi) + \frac{bV_1^2}{2}\cos(4\omega_{RF}t)$$

The phase-conjugated RF signal of the second term in (2.2) is shown as

$$V_2\cos(\omega_{RF}t + \varphi)^* \propto bV_1V_2\cos(\omega_{RF}t - \varphi) \tag{2.6}$$

The resulting phase conjugation applies across the entire array, resulting in retroreflection of the IF signal back towards the RF source. The higher frequency terms in (2.5) are undesired, non-phase-conjugated signals that are easily filtered and suppressed due to the large difference between frequencies.

B. Subharmonic Mixing Technique

In fundamental mixing, the squared term in (2.1) is used for phase conjugation. In subharmonic mixing, the third-order harmonic term cV^3 from (2.1) is used [25], [26]. The third term from the substitution of (2.2) into (2.1) becomes:

$$
\begin{aligned}
I_c = \frac{c}{4}\{&V_1^3\cos(3\omega_{LO}t)+V_2^3\cos(3\omega_{LO}t)\\
&+3V_1^2V_2[\cos((2\omega_{LO}+\omega_{RF})t+\varphi)+\cos((2\omega_{LO}-\omega_{RF})t-\varphi)]\\
&+3V_1^2V_2[\cos((\omega_{LO}+2\omega_{RF})t+2\varphi)+\cos((\omega_{LO}-2\omega_{RF})t-2\varphi)]\\
&+3(V_1^3+2V_1V_2^2)\cos(\omega_{LO}t)\\
&+3(V_2^3+2V_1^2V_2)\cos(\omega_{RF}t)\}
\end{aligned}
\tag{2.7}
$$

Using the term, $\left(\frac{c}{4}\right)3V_1^2V_2[\cos((2\omega_{LO}+\omega_{RF})t+\varphi)+\cos((2\omega_{LO}-\omega_{RF})t-\varphi)]$ from (2.7), the LO frequency can be set as the same as the RF frequency, $\omega_{LO} = \omega_{RF}$. The resultant is a signal

$$
\left(\frac{c}{4}\right)3V_1^2V_2[\cos(3\omega_{RF}t+\varphi)+\cos(\omega_{RF}t-\varphi)] \tag{2.8}
$$

The unwanted frequencies are suppressed and filtered, resulting in the phase conjugated signal of

$$
V_2\cos(\omega_{RF}t+\varphi)^* \propto \left(\frac{c}{4}\right)3V_1^2V_2\cos((\omega_{RF})t-\varphi) \tag{2.9}
$$

C. Quadruple Subharmonic Mixing Technique

The fundamental mixing technique uses a LO that is twice the frequency of the RF signal and the IF output signal is the phase-conjugated second-order harmonic term of the power series. The subharmonic technique outputs a higher-order harmonic and uses a LO source equal to the RF signal frequency. Both techniques have the disadvantage of requiring a high-frequency LO, which is sometimes impractical where dc power and budgets place restrictions on the design.

A quadruple subharmonic mixing approach was adopted in our system. From (2.1), the eV^5 term can be extracted from the substitution of (2.2) into (2.1) as similarly done for the bV^2 and cV^3 in (2.4) and (2.7) respectively. The resulting term for the output of the mixer can be described as

$$I_e \propto e \cdot \left[V_{LO}\cos(\omega_{LO}t) + V_{RF}\cos(\omega_{RF}t + \varphi)\right]^5 + \ldots$$

$$I_e \propto \frac{5e}{16}\left[V_{LO}{}^4 V_{RF}\cos\left((4\omega_{LO} - \omega_{RF})t - \varphi\right)\right] + \ldots \qquad (2.10)$$

From (2.10), $\omega_{IF} = 4\omega_{LO} - \omega_{RF}$. To obtain $\omega_{IF} = \omega_{RF}$ as done with the fundamental and subharmonic mixing, the required LO frequency has to be half of the RF frequency, $\omega_{LO} = \frac{\omega_{RF}}{2}$. The conjugate term becomes:

$$V_2\cos(\omega_{RF}t + \varphi)^* \propto \frac{5e}{16}\left[V_{LO}{}^4 V_{RF}\cos\left((\omega_{RF})t - \varphi\right)\right] \qquad (2.11)$$

Anti-parallel diodes suppress the second harmonic of the LO, which is at the same frequency of the RF and other odd-order mixing terms can be filtered out. The phase-conjugating operation through the quadruple subharmonic mixing further reduces the need for a high frequency LO source and has been adopted for use in the retrodirective satellite.

2.4 Retrodirective Circuitry

A. Mixer Array Design

The RF frequency, f_{RF} into the mixers is selected at 10.5 GHz. To distinguish between interrogated and retroreflected signal, the IF frequency, f_{IF} is selected to be 10.45 GHz. The relationship changes between RF and IF frequencies as mentioned in Section 2.3C. From (2.10), the IF and RF frequencies are substituted into $f_{IF} = 4f_{LO} - f_{RF}$ and the LO frequency can be solved, resulting in

$$10.45GHz = 4f_{LO} - 10.5GHz$$

Solving for f_{LO} results in

$$f_{LO} = 5.2375\,\text{GHz}$$

A typical mixer has three ports, one dedicated to the RF, IF and LO signals, Fig. 2.5 (a). Fig. 2.5 (b) shows a block schematic of an individual quadruple subharmonic mixer using Agilent HMS-8202 anti-parallel diodes. The RF signal and the IF signal share the same port. The mixer circuitry includes a RF blocking band stop filter preventing the RF signal from reaching the LO source and a LO band stop filter blocking leakage of the LO signal. Input and output matching networks match the impedance of the mixer to connecting circuits and help minimize conversion loss. The microstrip filters and matching networks are printed on Rogers TMM4 substrate (εr=4.5, h=0.0381 cm).

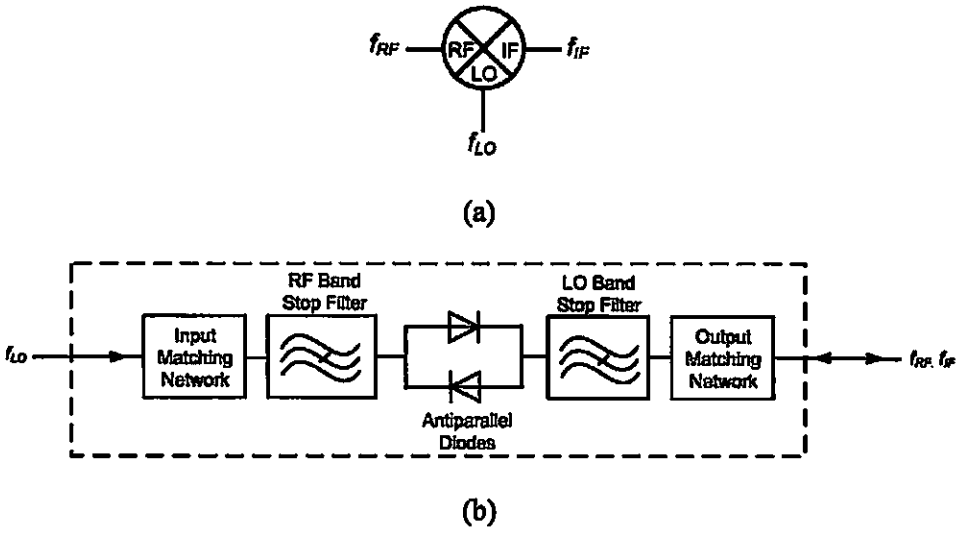

Fig. 2.5: (a) Basic mixer circuit, (b) Block diagram of quadruple subharmonic mixer consisting of a LO input matching network, an RF bandstop filter, anti-parallel diodes, LO bandstop filter, and RF output matching network

A feeding network power divider was designed to distribute equal LO power to all mixer elements. This Wilkinson power divider was selected to provide the best isolation between the mixers. Eight mixer elements are attached to the feeding network resulting in the fabricated mixer array shown in Fig. 2.6 (a).

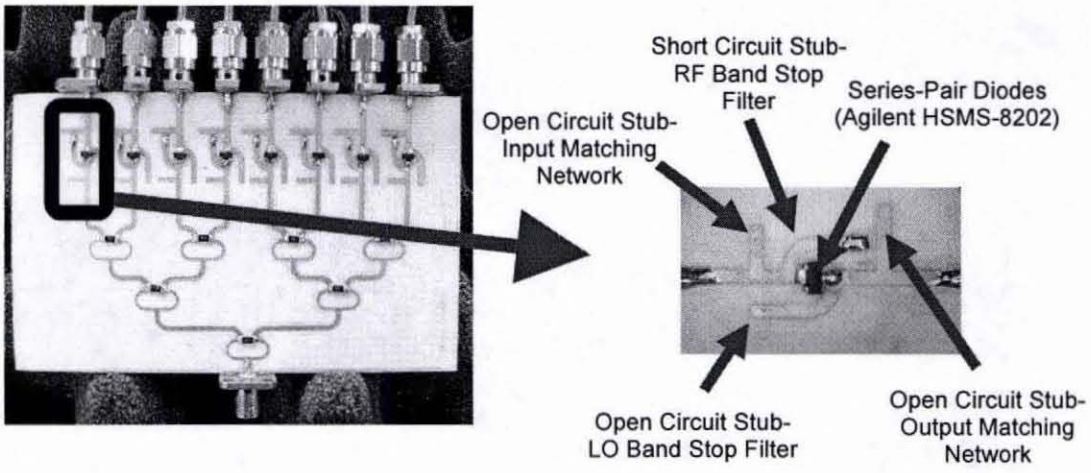

(a) (b)

Fig. 2.6: (a) 8 Element mixer array, (b) Single mixer

The measured isolation of a single mixer between the IF and fundamental LO is 65 dB. The second harmonic of the LO is rejected and measured to be 55 dB smaller than the IF signal. The average measured conversion loss of the quadratic subharmonic mixer in the array is 26 dB.

B. Antenna Array

The antenna array design determines the steering capability of the retrodirective satellite. As more elements are implemented in the array the beam width of the signal narrows. The retrodirected beam could be more focused with a larger array. However circuit size and power limitations constrain the design.

The antenna element is a square microstrip patch designed to cover 10.45 GHz to 10.5 GHz. The patch is mitered at opposite ends to achieve two slightly different resonant modes [27]. Circular polarization is achieved when the two modes are

orthogonal to each other and 90° out of phase (Fig. 2.7). The antenna is fabricated on Rogers TMM3 substrate (εr=3.27, h=0.0635 cm).

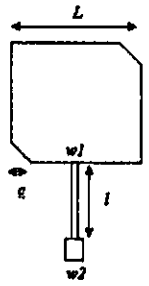

Fig. 2.7: Patch antenna element with dimensions L = 0.762 cm, c = 0.102 cm, w1 = 0.0457 cm, l = 0.541 cm, w2 = 0.150 cm.

The return loss of a single patch is shown in Fig. 2.8. The axial ratio (AR) is the ratio of co-polar and cross-polarization in a one-dimensional plane. Ideally the AR should be relatively the same for both E and H planes of the antenna. The simulated and measured AR is shown in Fig. 2.9 and Fig. 2.10 both E and H planes respectively. The discrepancies between measured and simulation values depicted in the AR patterns are a result of the reflective environment the antennas were tested in. The sensitive nature of the axial ratio test requires test conditions obtainable in an anechoic chamber.

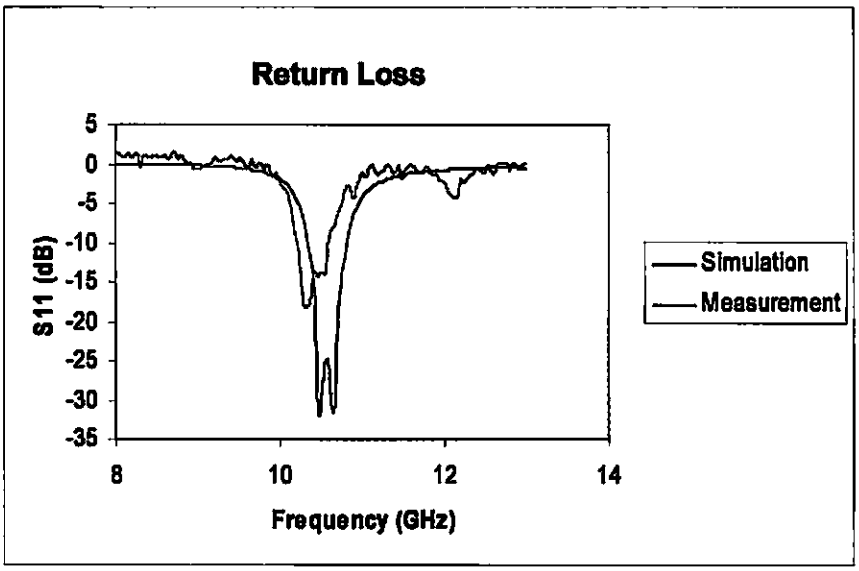

Fig. 2.8: Reflection Coefficient of patch antenna

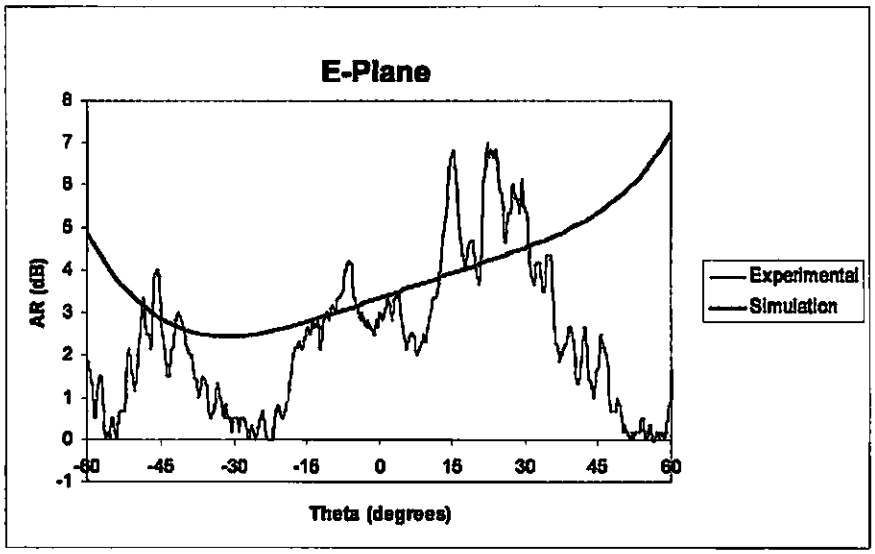

Fig. 2.9: E-plane simulated (Ansoft Ensemble) and experimental Axial Ratio (AR) of individual patch antenna

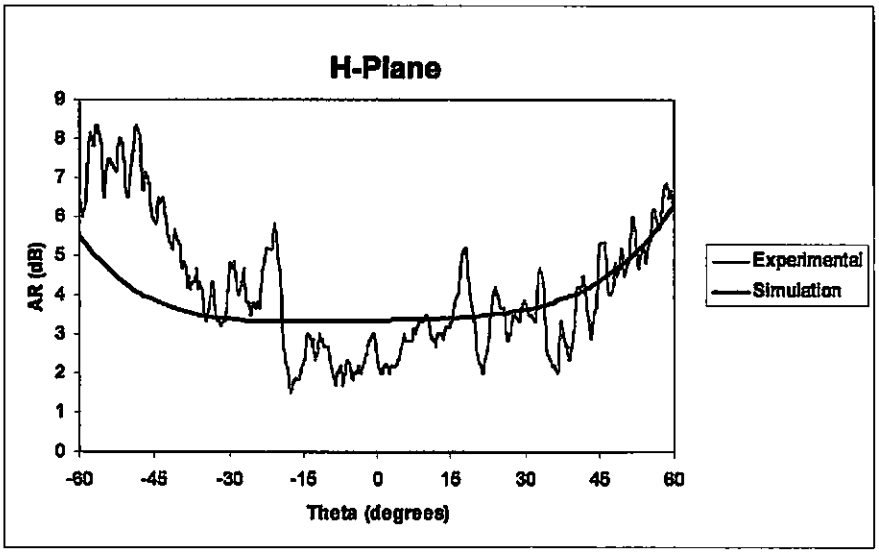

Fig. 2.10: H-plane simulated (Ansoft Ensemble) and experimental AR of individual patch antenna

Significant retrodirectivity requires an array of at least four elements per dimension. Conventionally, this is achieved with a 4 x 4 array layout. To reduce circuit size and required feed power, a cross-shaped array consisting of four elements in two orthogonal dimensions was used instead, reducing the amount of elements from 16 for the conventional array to eight elements. The array spacing is $0.484\lambda = 1.383$ cm between elements (Fig. 2.11). With this configuration the array should be able to exhibit retrodirectivity in any direction. The antenna array is attached to mixer array depicted in Fig. 2.12.

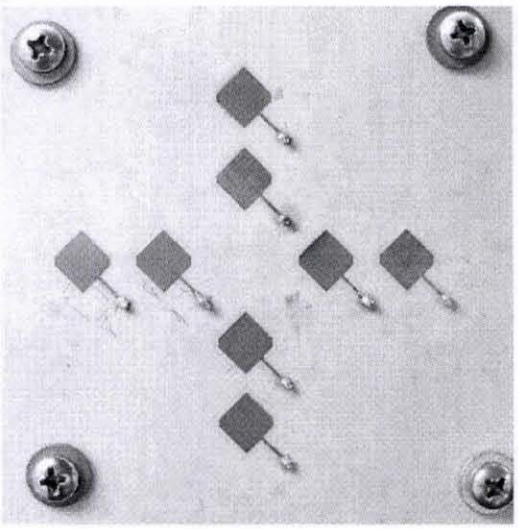

Fig. 2.11: Circularly polarized cross-shaped microstrip patch antenna array designed using RPDesign and Ansoft Ensemble. The resonant frequency is 10.5 GHz.

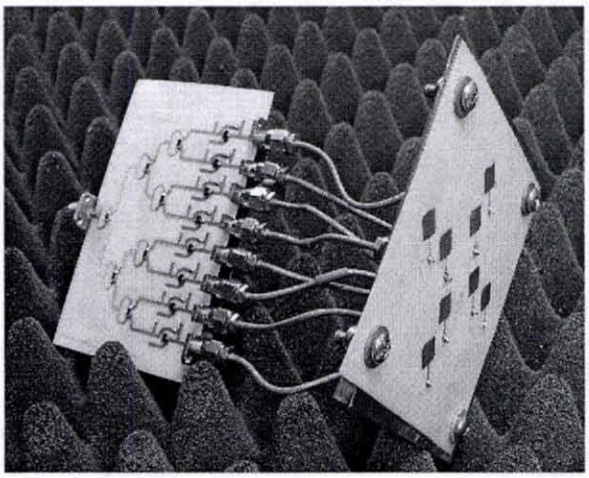

Fig. 2.12: Photograph of antenna and mixer array

C. Oscillator

Where possible, commercial-off-the-shelf components are selected to reduce complexities in design and to meet component requirements for space. These parts

include the local oscillator for both interrogator and retrodirective systems and various connectors.

The dielectric resonator oscillators (DROs) purchased from Hurley-CTI for the 10.5-GHz interrogator and the 5.2375-GHz LO source for the retrodirective array are space rated, remaining stable in the temperature range of space. The mechanical tuning in the DRO allowed modification for slight frequency shifts in other circuitry. The picture of the oscillator is shown in Fig. 2.13.

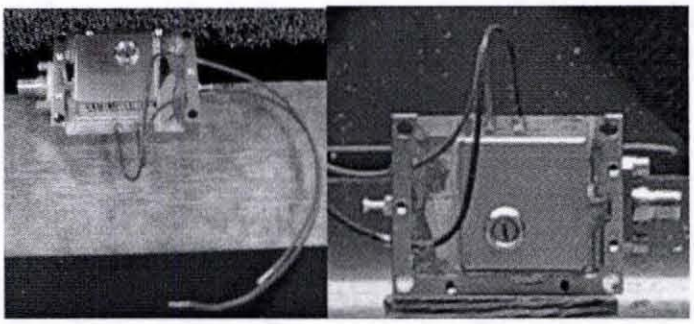

Fig. 2.13: Pictures of the Oscillator.

2.5 Interrogator and Receiver Circuitry

In this retrodirective system, the received signal is a function of the interrogator's signal power. Thus, the interrogator must produce a signal powerful enough so that the retroreflected signal is recoverable by the receiver. The received signal is then converted to an analog voltage that is then transmitted to a ground station.

Fig. 2.14(a) shows the communication link between the two nanosatellites. The interrogator transmits a 10.5-GHz monotone signal and is received by the retrodirective array system on the other satellite. A 10.45-GHz signal is retroreflected from the retrodirective array and received by the interrogator satellite. The interrogator and

receive antennas on the transponder satellite use the same patch antenna as the elements used in the retrodirective antenna array.

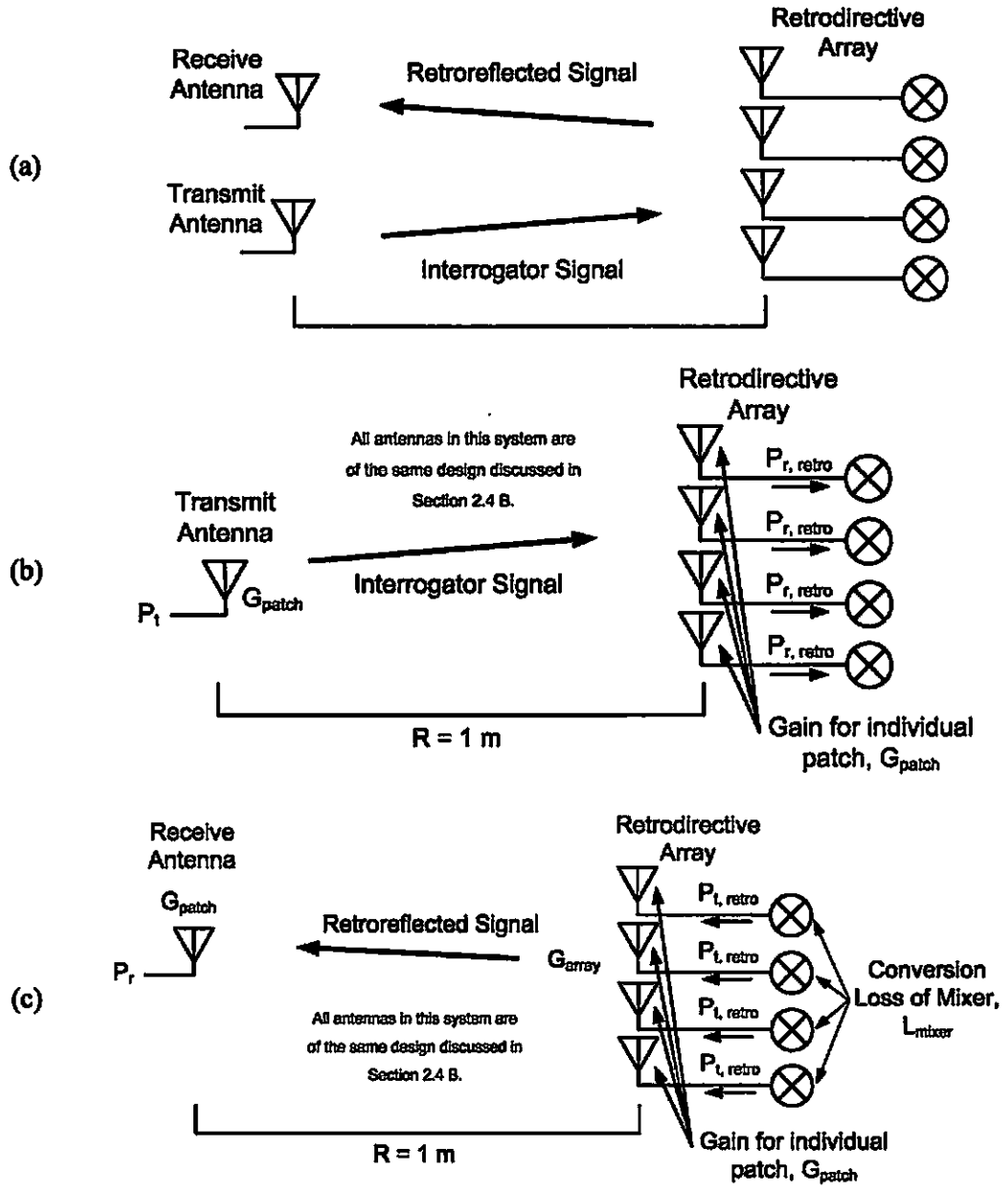

Fig. 2.14: (a) Communication link between retrodirective array and interrogator, (b) Path for interrogator signal, $P_{r,retro}$ is calculated, (c)Path for retrodirected signal, P_r is calculated from this path.

Although the differences in transmit and receive frequencies are not essential to the retrodirectivity process, it does allow one to distinguish between the two signals in the laboratory. The returned signal at 10.45 GHz must be strong enough after downconversion to be detected. The power received by the interrogator can be calculated by following the path of the signal from the interrogator antenna (Fig. 2.14). P_t is the output power of the interrogator source, G_{patch} is the gain of the patch antennas, L_{mixer} is the conversion loss of the phase-conjugating mixer, and G_{array} is the gain of the phase-conjugating array. Using the Friis transmission formula, the power received at each element in the retrodirective array (Fig. 2.14(b)) is

$$P_{r,retro} = \left(\frac{1}{4\pi R^2}\right) P_t G_{patch} \left(\frac{\lambda^2}{4\pi} G_{patch}\right) \tag{2.12}$$

The power transmitted by the retrodirective array is affected by the individual mixer conversion loss and the results in

$$P_{t,retro} = P_{r,retro} \cdot L_{mixer} = \left(\frac{1}{4\pi R^2}\right) P_t G_{patch} \left(\frac{\lambda^2}{4\pi} G_{patch}\right) L_{mixer} \tag{2.13}$$

The power received at the receiver antenna is dependent on the power transmitted by the retrodirective array (Fig. 2.14(c)), and the gain of the receiving patch element is given by

$$P_r = \left(\frac{1}{4\pi R^2}\right) P_{t,retro} \cdot G_{array\_total} \left(\frac{\lambda^2}{4\pi} G_{patch}\right) \tag{2.14}$$

The gain of the retrodirective array, G_{array_total} is dependent on the gain of the individual patch antenna elements, G_{patch} and the gain associated with the array factor (AF), G_{array} resulting in $G_{array\_total} = G_{array} \cdot G_{patch}$. Substituting G_{array_total} and (2.13) into (2.14) results in

$$P_r = \left(\frac{1}{4\pi R^2}\right)\left(\frac{1}{4\pi R^2}\right) P_t G_{patch}\left(\frac{\lambda^2}{4\pi} G_{patch}\right) L_{mixer} \cdot G_{array} \cdot G_{patch}\left(\frac{\lambda^2}{4\pi} G_{patch}\right) \quad (2.15)$$

Simplifying (2.15) gives

$$P_r = \left(\frac{1}{4\pi R^2}\right)^2 P_t G_{patch}\left(\frac{\lambda^2}{4\pi} G_{patch}\right) L_{mixer} G_{array} G_{patch}\left(\frac{\lambda^2}{4\pi} G_{patch}\right) \quad (2.16)$$

The interrogator oscillator output, the frequency, communication distance, conversion loss of the mixers, patch antenna gain, and array gain are all known parameters, which allow us to find the actual received power by the interrogator front end about -100 dBm. The minimum detectable power for the detector is -60 dBm. Therefore the receiver circuit should be designed so that it can provide 40 dB gain. The system schematic is shown in Fig. 2.15.

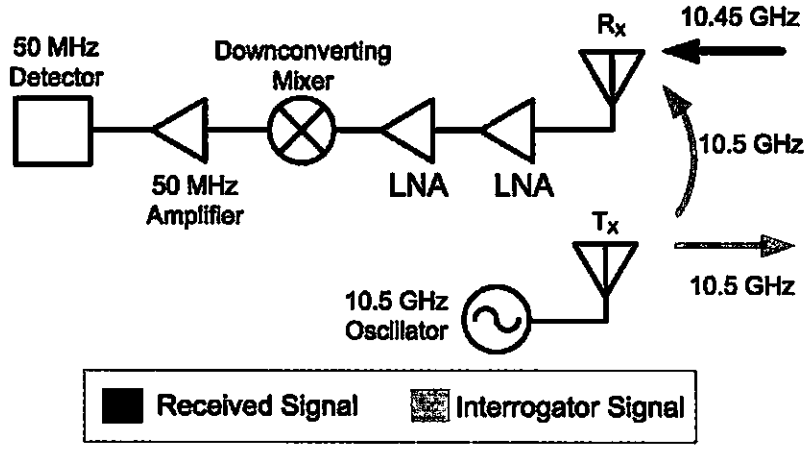

Fig. 2.15: Schematic of Receiver Circuitry. Interrogator transmits 10.5 GHz signal (T_X). Receiver mixes 10.45 and 10.5 GHz (R_X) and produces a downconverted signal at 50 MHz.

To conserve dc power, space, and other limited resources aboard the 1500-cubic-cm nanosatellite, a separate local oscillator (LO) for the receiver was eliminated from the

design. As mentioned in Section 2.4 A, typical mixers have dedicated LO ports. Instead, the mixer is designed with the RF signal and IF signal sharing the same port. The LO signal for the receiver is coupled off from the interrogator via the patch antennas of the interrogator and receiver. This antenna-coupling scheme eliminates the need for a power divider. The distance between the antennas is optimized so that the LO power for the mixer is 0 dBm after a two-stage amplifier. The mixing of the two signals produces a 50-MHz downconverted signal. Because a diode mixer is used, an amplifer following the mixer compensates for conversion losss. Based on the link budget, a prototype system was fabricated using commercial-off-the shelf parts. Components in the interrogator/receiver were carefully chosen based on constraints such as size, weight, cost, and reliability. Fig. 2.16(a) shows the single-board design consisting of a two stage amplifier circuit, downconverting mixer, 50-MHz amplifier, and the power detector. The receiver circuitry is then connected to the corresponding antennas. A two-stage amplifier was designed using internally matched Agilent MGA 86576 LNAs to amplify the retrodirected signal and coupled LO power by 17 dB.

The mixer was designed using an Agilent 8202 Schottky diode (Fig. 2.17), resulting in a 10 dB conversion loss. The optimal LO power into the mixer is approximately 0 dBm. To achieve this, the distance L between the receiver and interrogating antennas was calibrated (Fig. 2.16(b)).

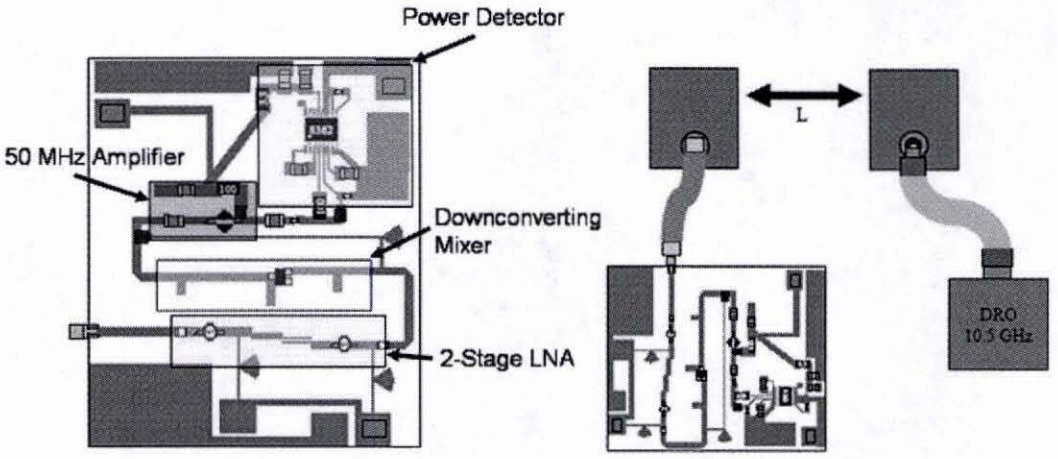

Fig. 2.16: (a) Receiver circuit board layout, (b) Interrogator and receiver connected to coupled patch antennas.

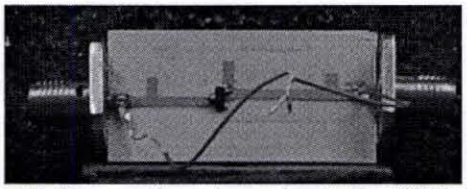

Fig. 2.17: Downverting mixer using Agilent 8202 diode

The downconverted signal is boosted by a 50-MHz amplifier with 30 dB gain which was designed using a MiniCircuits ERA-8SM, providing the detector sufficient power for detection. The Analog Devices AD8362 detector was selected for its frequency characteristics and sensitivity. The detector was biased for 50 MHz signals and is capable of detecting down to -60 dBm. The detector outputs a linear analog voltage corresponding to the RF power in dBm (0.05 V per dB). Fig. 2.18 shows the completed receiver satellite.

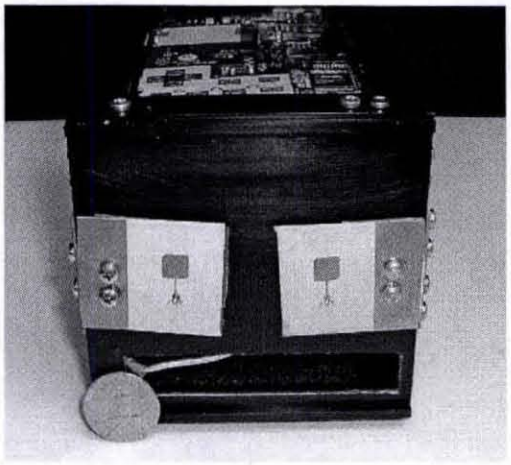

Fig. 2.18: Picture of coupled patched antenna mounted on satellite

2.6 Retrodirective Characterization

To quantify retrodirective performance, two types of measurements are made. The first measurement is the bistatic radar cross section (RCS) [28]. The bistatic RCS characterizes the steering performance of the retrodirective array in a controlled lab environment. The second measurement is the monostatic RCS and demonstrates overall system performance simulating communication between an transponder system and the retrodirective counterpart.

In the bistatic RCS measurement the receiver is placed on a computer-controlled rotating arm, while an interrogator source horn is fixed at a specific location from the retrodirective circuitry (Fig. 2.19). The retroreflected signal power is measured as the arm sweeps the receiver from -60° to +60°.

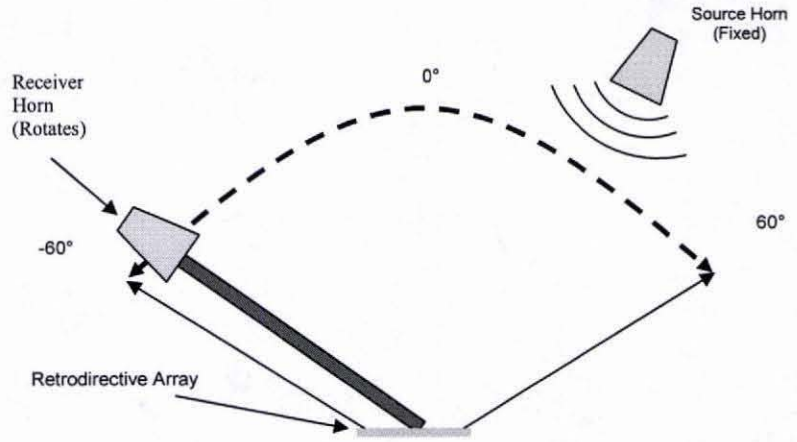

Fig. 2.19: Bistatic RCS setup

The expected measurement exhibits beam forming in the direction of the source. The horns are configured to measure the radiation patterns in the co-polar and cross-polar planes. Because the individual antenna elements are designed for circular polarization, both co-polar and cross-polar RCS patterns should be similar.

The next measurement is the monostatic RCS. In this measurement the interrogator and receiver are collocated and placed on the one meter computer-controlled arm, Fig. 2.20. Sweeping interrogator and receiver horn from -60° to +60° simulates the interrogator/receiver satellite's communication link with the retrodirective satellite.

The receive horn measures the power of the IF signal being produced by the retrodirective array. The retrodirective array should instantaneously track the interrogator signal resulting in a constant power at the receiver horn.

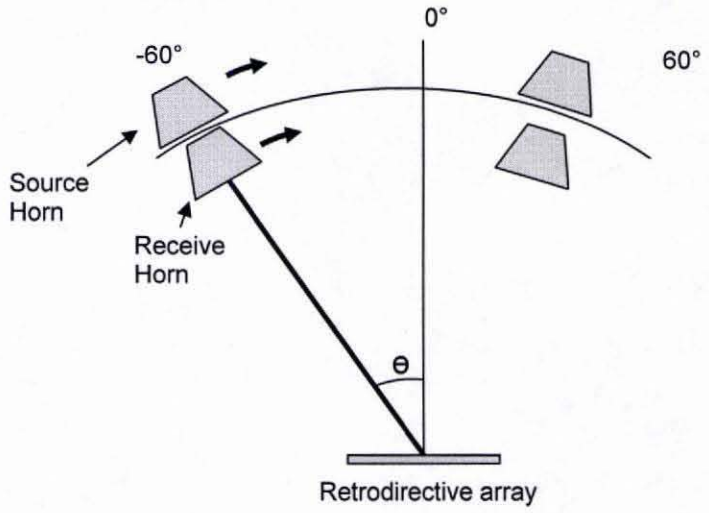

Fig. 2.20: Monostatic RCS setup

2.7 Experimental Results

The hardware was tested in a methodical manner. The first step in the testing procedure involves measuring the performance of the retrodirective array before installation in the satellite bus. Two-dimensional steering is confirmed and demonstrated in Section 2.7.1.

The second part of the procedure, Section 2.7.2, the retrodirective hardware has been integrated into the satellite bus. Onboard processors control the retrodirective array and the system is tested once again before communicating with the transponder satellite. After confirmation the retrodirective circuitry is properly working, the communication link is established between the two satellites. The received power of the communication

link is measured over a predetermined period of time. The data is recorded and transferred from the transponder satellite to the ground station.

2.7.1 Two-dimensional Measurements

The array is tested outside of the satellite bus. A bistatic RCS is taken along the diagonal axis of the antenna array (Fig. 2.21). Testing along this axis demonstrates two-dimensional self-steering capabilities. Three measurements are taken, with the interrogator horn is placed at -20°, 0° and +20°. The array demonstrated two-dimensional self-steering of the beam to each of the interrogator sources, shown in Fig. 2.22, Fig. 2.23, and Fig. 2.24.

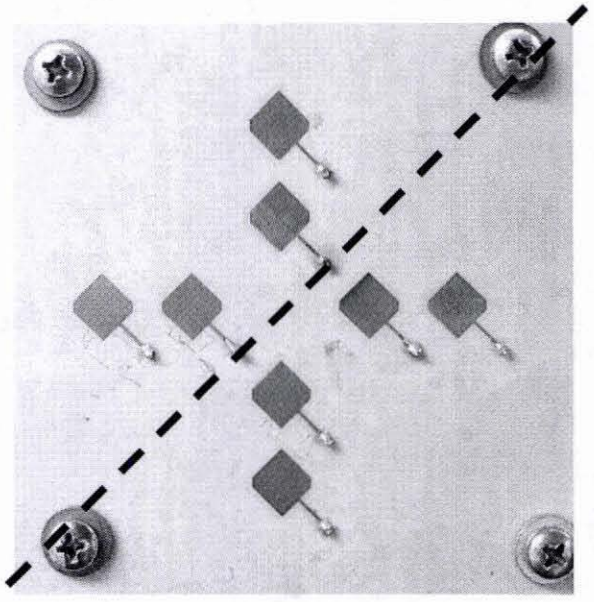

Fig. 2.21: Bistatic RCS taken along 45° plane of antenna array

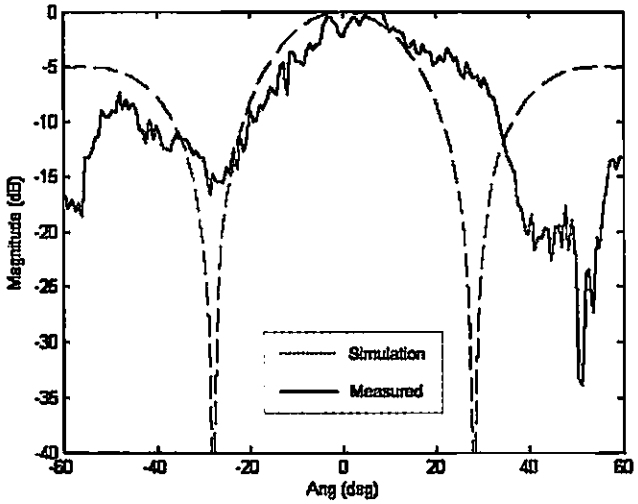

Fig. 2.22: RCS of the retrodirective array with source horn at 0°, measured RCS matches simulated RCS and power directed at 0°.

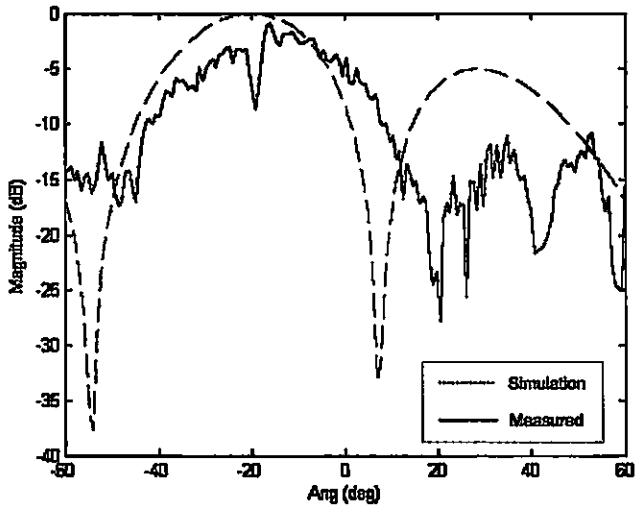

Fig. 2.23: RCS of the retrodirective array with source horn at -20°, measured RCS matches simulated RCS and power directed at -20°.

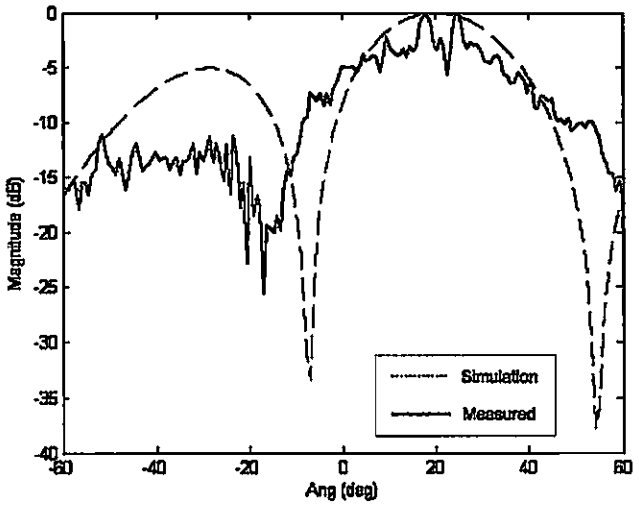

Fig. 2.24: RCS of retrodirective array with source horn at +20°, measured RCS matches simulated RCS and power directed at +20°.

The RCS patterns in the diagonal cross section correlates well with the simulated radiation patterns. The strong correlation between simulated and measured RCS patterns identifies proper retrodirectivity of the interrogated signal. The retrodirective array was powered by external lab equipment and produced the RCS patterns in Fig. 2.22, 2.23, and 2.24. The retrodirective array was integrated into the satellite bus and the performance of the retrodirective array is reevaluated in Section 2.7.2.

2.7.2 Continuous Wave Power Measurements

Section 2.7.1 measured the performance of the retrodirective array using lab equipment. In this section, the hardware is mounted into the satellite bus and the retrodirective array is powered and controlled by onboard circuitry. Before a communication link is established between transponder and retrodirective satellites, the

retrodirective satellite is individually tested by taking bistatic and monostatic RCS measurements.

A. Bistatic Measurements

The measurements presented are the bistatic RCS of the retrodirective array integrated into the satellite bus. This section's measurements differ from section 2.7.1 measurements because the retrodirective array is powered and controlled from the satellite bus and not manually powered by lab equipment. The first RCS measurement uses a horn antenna as a source and is fixed at broadside, 0°. The power is measured by the sweeping receive horn and is centered at 0° Fig. 2.25. In the second and third measurements, the source horn was placed at +20° and -20°. In both cases the peak power was located at the source angle Fig. 2.26 and 2.27.

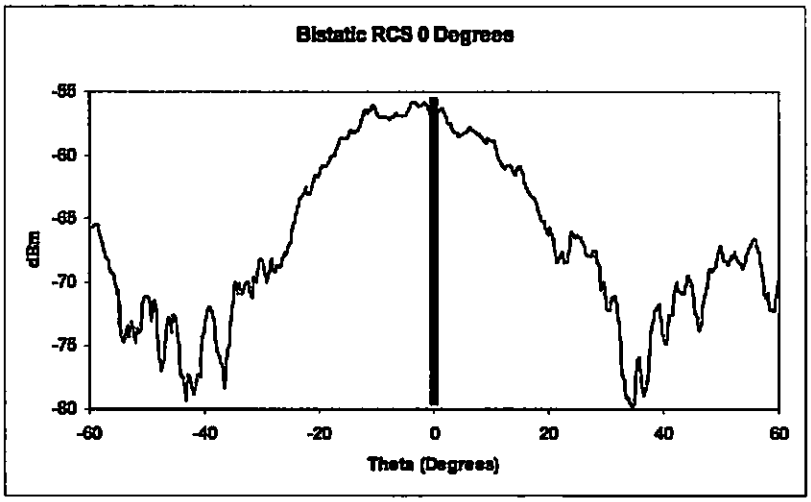

Fig. 2.25: Bistatic RCS where interrogator is placed at 0°, retroreflected power directed at 0°

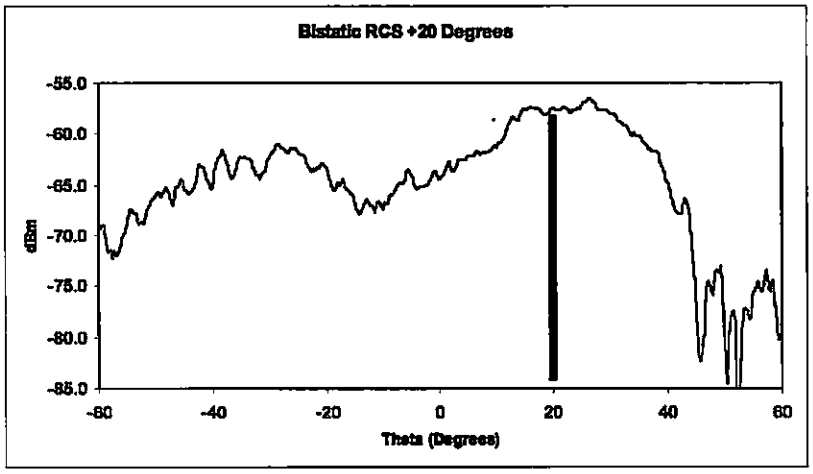

Fig. 2.26: Bistatic RCS where interrogator is placed at +20°, retroreflected power directed at +20°.

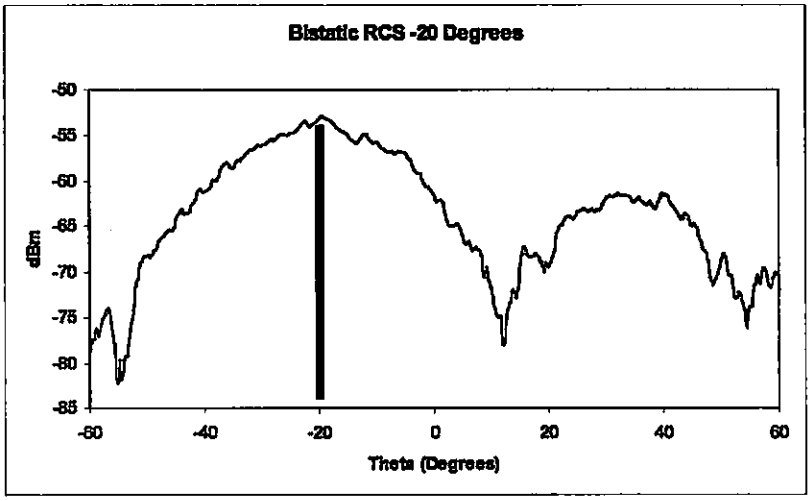

Fig. 2.27: Bistatic RCS where interrogator is placed at -20°, retroreflected power directed at -20°.

The bistatic RCS patterns demonstrate the retrodirective array in the satellite bus properly steers the beam to the interrogator source. The graphs show the difference between the main and side lobes of 10 dBm.

B. Monostatic Measurements

Fig. 2.28 depicts the monostatic RCS. Two horn antennas for the interrogator source and receiver simulate the transmit and receive antennas on the transponder satellite. The range in which a detectable retrodirected signal is received is shown by the vertical lines on the graph from -40° to +40°. Fig. 2.29 shows the monostatic RCS pattern of a fixed array without retrodirective circuitry. When compared to the retrodirective monostatic pattern, it is observed that the range in which maximum power of the IF signal is detected increases by four.

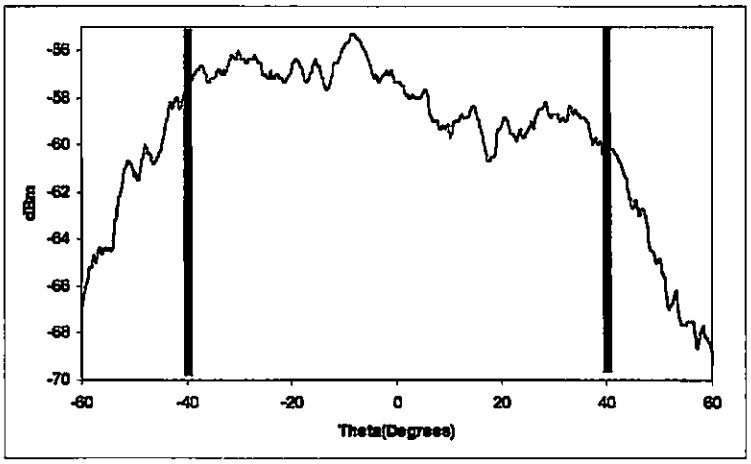

Fig. 2.28: Monostatic RCS of the retrodirective array, retrodirective array demonstrates steering range of -40° to 40°.

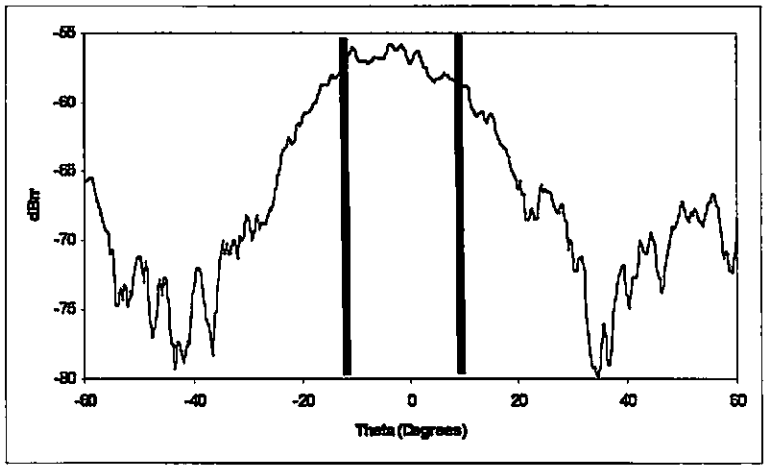

Fig. 2.29: Fixed beam RCS of antenna array, beam width of -10° to 10° compared to range of retrodirective array in Fig. 2.28.

C. *Interrogator/Receiver Measurements*

The monostatic RCS patterns reviewed in the previous section simulates the relationship between retrodirective satellite and interrogator satellite. The communications link between interrogator and retrodirective systems was tested after both systems are integrated with the satellite's system bus. The two satellites are placed one meter apart. The transponder satellite sweeps from -60° to +60° and the receiver detects the power of the IF signal being received from the retrodirective satellite and records the DC voltage output (Fig. 2.30) .

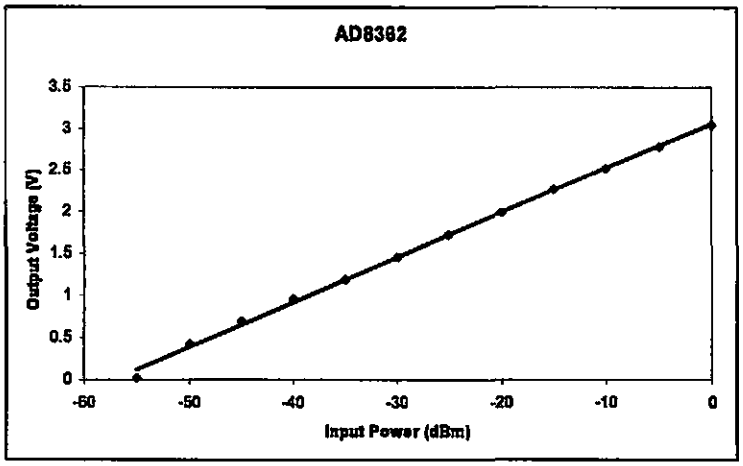

Fig. 2.30: Voltage output of the power detector as a function of input power.

The monostatic radiation pattern shows a substantial signal is being received in the range of -40° to +40° (Fig. 2.31) as the voltage outputted by the power detector onboard the transponder satellite. Similarities are observed by comparing the measurements mentioned in the previous section to the RCS pattern taken by the transponder satellite. Correlation between Fig. 2.28 and Fig. 2.31 confirms the retrodirective link range between two satellites. Satellite communication between two satellites is established and maintained without a priori knowledge of the positions of the other satellites within the network.

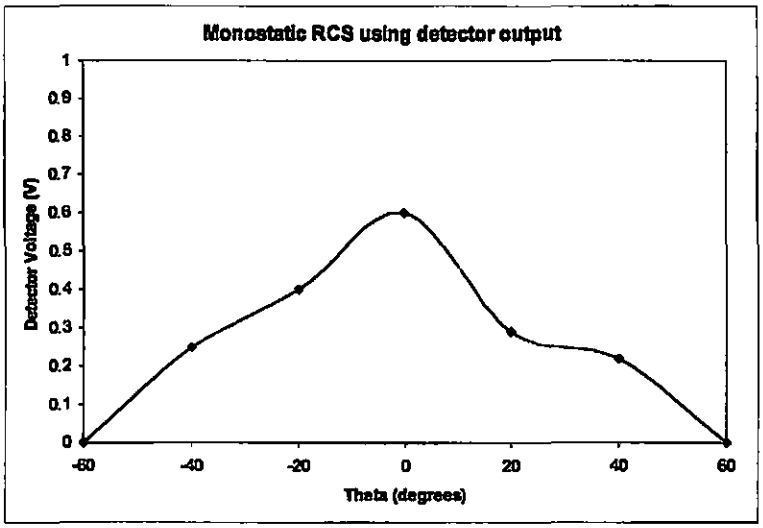

Fig. 2.31: Monostatic RCS using detector output voltage

The monostatic RCS measured by the transponder satellite demonstrates a retrodirective link between a pair of small satellites. In satellite-to-satellite communications it would be ideal for both satellites to incorporate retrodirective antennas. Fig. 2.32 shows a retrodirective to retrodirective communication link. The demonstrated retrodirective array discussed in this chapter produces a retroreflected signal as a function of the incoming interrogated signal and is subject to conversion loss. By adding gain to the retrodirective array compensates for the conversion loss and provides sufficient signal strength for signal reception at the interrogator source.

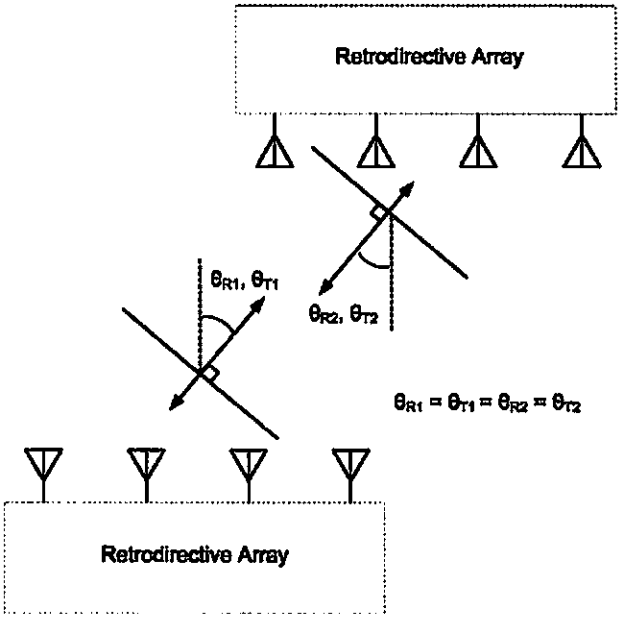

Fig. 2.32: Retrodirective to retrodirective link

CHAPTER 3

FREQUENCY-CONTROLLED PHASED ARRAYS[3]

3.1 Introduction

The frequency-controlled array introduced in Section 1.2*C* expands on the frequency-scanned array design by using heterodyne mixing at each element to keep a constant transmit and receive frequency (Fig. 3.1). The frequency-controlled phased array provides many desirable beam steering characteristics of conventional arrays without complex circuitry and the high cost associated with phase shifters. The simple control of the frequency-controlled array allows for easy integration with current systems. A perfect application of the frequency-controlled array is integration with the M2C2 Humvee which uses GPS. The GPS system provides precise tracking of the target communication satellite and provides accurate steering of satellite dish/antenna. The frequency-controlled phased array steers in real time addressing the limited tracking speed of a mechanical driven satellite dish.

[3] Portions of this chapter have been published in [29]

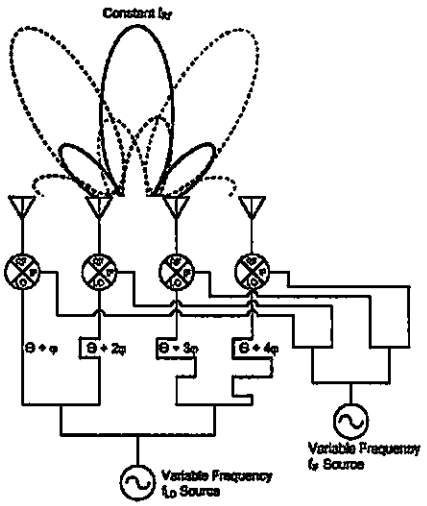

Fig. 3.1: General heterodyne-scan phased-array architecture used in [7]-[10]. Two VCOs are required to maintain a constant RF.

Several successful demonstrations based on this heterodyne phased-array system have been reported. The first was an eight-element X-band array using a corporate LO feed network, a series IF feed network, and microstrip patch antennas [7]. Researchers at UCLA subsequently demonstrated a Ka-band array with improved bandwidth and amplitude balance by replacing the microstrip patches and series IF feed network with wideband radiating elements and a corporate IF feed network, respectively [8]-[10].

This chapter demonstrates the following features:

- The work cited above requires the adjustment of both an LO and IF VCO to maintain a constant RF frequency. This chapter demonstrates a circuit requiring the use of only one VCO based on [5], without the complexities associated with a three-oscillator phase-locked loop as described in [30].

- Previously reported heterodyne phased arrays operated in transmit mode only. This chapter presents a transmit/receive array that can operate in full-duplex mode.
- The LO corporate feed network in Fig. 3.1 can become quite unwieldy for large arrays. This chapter demonstrates a novel series-feed network that is more compact than a corporate feed. The design allows each mixer to be pumped with an equal level of LO power, resulting in less than 3-dB amplitude variation over the steering range.

3.2 One-Dimensional Full-Duplex, Voltage-Controlled Phased Array

3.2.1 Design Parameters

Fig. 3.2 illustrates the system proposed in this chapter that differs from Fig. 3.1 in several respects. First of all, there are two sets of arrays: one four-element array for transmission, and a second array for reception, allowing full-duplex operation. Secondly, it is unnecessary to adjust both an LO and IF source to maintain a constant RF. In our architecture, the second VCO is replaced by a fixed-frequency source operating at f_{RF}. The only expense is the additional mixer A, but it is less expensive than a VCO – a small price for having the steering control based solely on the tuning voltage of a single VCO. Connected to Mixers A are fixed-frequency oscillators that oscillate at f_{RF}. The output of Mixers A is thus f_{RF}-f_{LO}. This intermediate frequency signal is then routed to the mixer array, whereupon they are mixed with f_{LO}, resulting in f_{RF} appearing at the antenna elements.

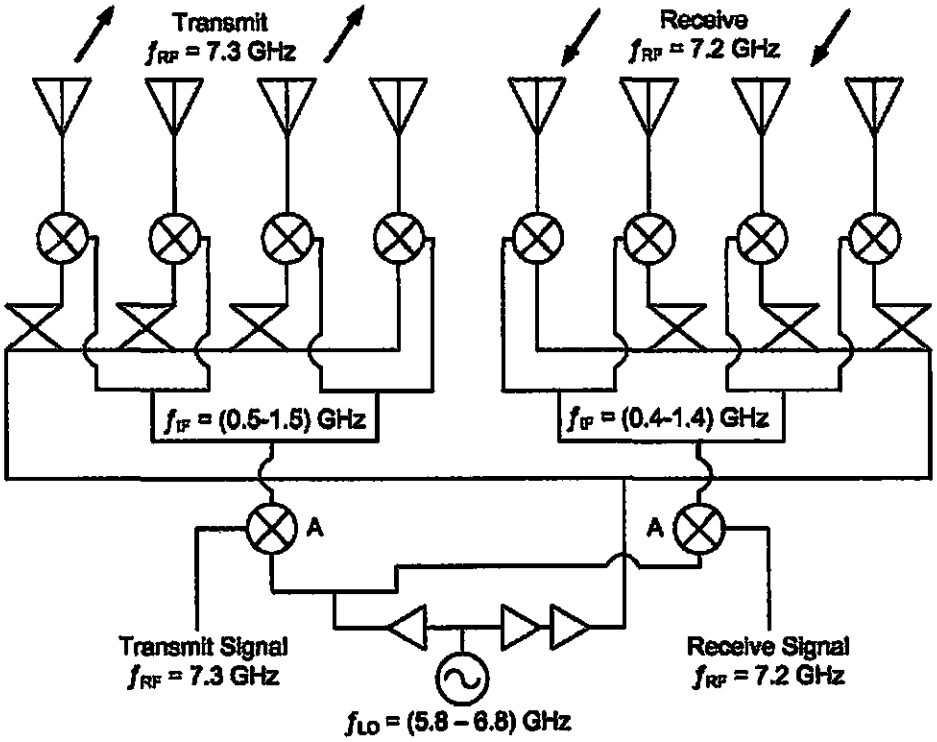

Fig. 3.2: Full-duplex frequency-controlled phased-array architecture. Only one VCO is required for beam control.

The f_{RF} source feeding Mixer A can remain fixed at that frequency for a single-channel system, or may be tuned to some other frequency in the case of a frequency-division multiple access system.

For the purposes of testing our array as both a transmitter and receiver in full-duplex mode, the RF signal transmitted by the array is set to 7.3 GHz, while the received signal is set to 7.2 GHz. In principle, however, both the transmit and receive frequency can remain the same.

A photograph of the complete system is shown in Fig. 3.3. Note that this is a modular breadboard model in which each module is characterized prior to being

integrated with each other. In a real system, there would not be SMA interconnects between modules.

3.2.2 One-Dimensional Frequency-Controlled Circuitry and Design

A. Antenna and Mixer Arrays

The radiating-edge-fed patch antennas in Fig. 3.3 are fabricated on RT/duroid 5880 substrate (thickness 0.7874 mm, εr = 2.2). The antennas are connected to Hittite HMC220MS8 mixers with operating RF/LO frequencies ranging from 5-12 GHz, and an IF frequency range of DC-4 GHz. As shown in Figs. 3.2 and 3.3, the mixers are connected through vias to IF corporate feed networks using Wilkinson power dividers. The feed networks and mixer arrays are fabricated on RT/duroid 6010.2LM substrate (thickness 0.635 mm, εr = 10.2).

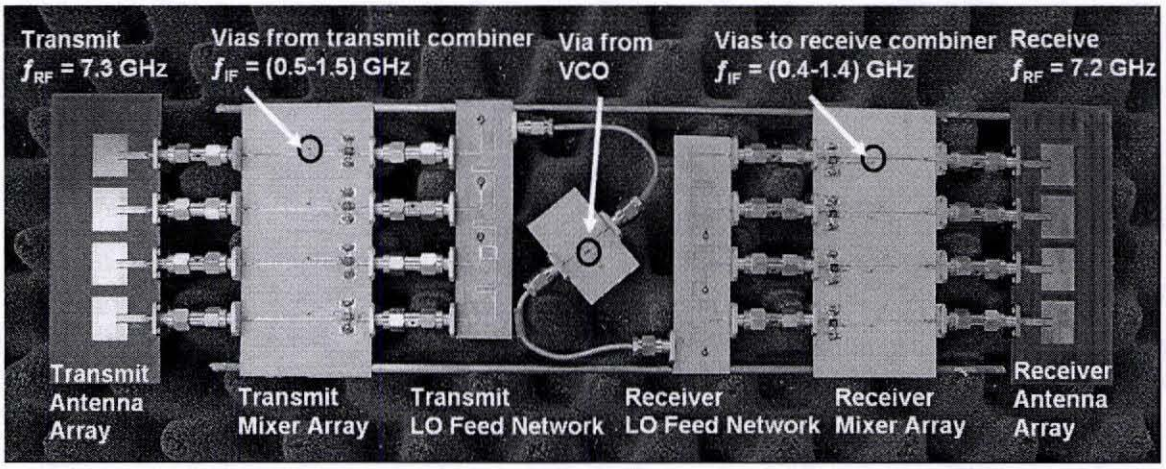

Fig. 3.3: Transmit and receive phased array. Vias connect to the VCO and transmit/receive feed networks.

B. Phase-Delay LO Feed Network

The most straightforward way of implementing a phase-delay LO feed network is to use transmission lines of differing lengths. Fig. 3.1 shows a typical network of this type, in which adjacent lines have successive phase shifts with $\phi=2n\pi$ for broadside radiation at the VCO's center frequency. The disadvantage of such networks is that it takes up considerable space, and the longer line lengths result in higher loss, resulting in amplitude variations across the steering range. This is the type of network that was used in [3]-[5].

An alternative delay network is the one in [2], which consists of one transmission line with coupled-line taps to each mixer. In that paper, each coupled-line section has the same amount of coupling, leading to an unequal mixer conversion loss for each element. The phase-delay LO feed network proposed here is also series fed, but unlike the taps used in [2], successive branchline couplers are designed to tap off a varying amount of power, resulting in an even distribution of LO power to each mixer in the array.

G. Shiroma, co-member of this project, designed the phase-delay LO network. Fig. 3.4 shows the fabricated four-element phase-delay LO feed network with a progressive phase shift of $\phi = 4\pi$ at 6.3 GHz.

For a lossless network, there would be a 6-dB insertion loss at each of the four ports. Fig. 3.5 shows that between 5.8-6.8 GHz, the measured insertion loss at each port is 8 ± 2.5 dB. The imbalance between ports is remedied by applying sufficient LO power to ensure that the mixers receive the minimum required power, while assuming a worst case LO network loss of 10.5 dB. Applying more than the minimum LO power to the mixers results in only a minimum change in mixer performance.

The measured phase response of the LO feed network is shown in Fig. 3.6. As expected, the phases of the four ports are equal at the center frequency of 6.3 GHz. At other frequencies, the progressive 4π delay lines create the phase progression required for beam steering.

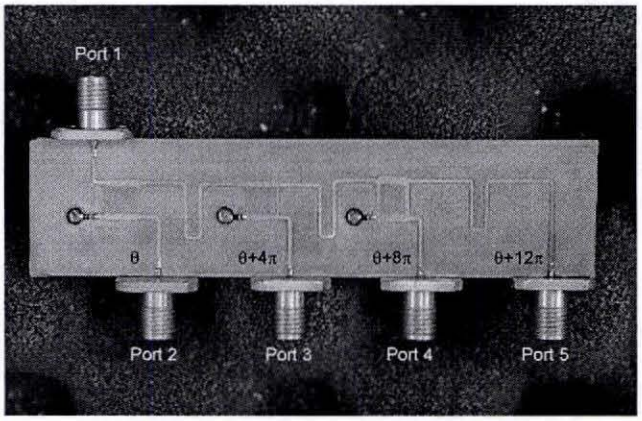

Fig. 3.4: Four-element LO feed network with a progressive phase delay of $\phi = 4\pi$. The network is fabricated on RT/duroid 6010.2LM substrate (thickness 0.635 mm, $\varepsilon r = 10.2$).

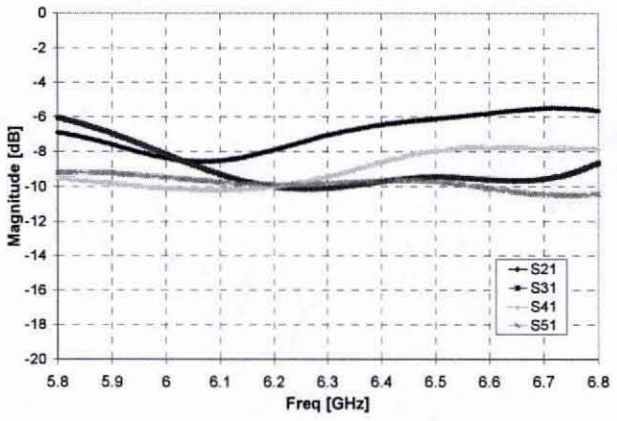

Fig. 3.5: Measured insertion loss of the four-element LO feed network.

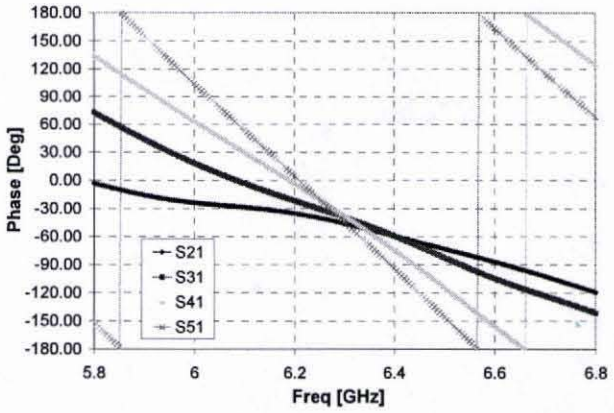

Fig. 3.6: Measured phase response of the 4-element LO network.

C. Transmitter, Receiver, and VCO Circuitry

Fig. 3.7 shows the remainder of the system, consisting of transmitter, receiver, and VCO circuitry. The VCO is a Hittite HMC358MS8G. Since the LO is split tenfold, Hittite HMC407MS8G power amplifiers are added to ensure 10 dBm reaches each mixer. Lowpass filters are added to the IF ports of the transmit and receive mixers. Since the RF-to-LO isolation was not sufficient to suppress the LO signal, a stepped-impedance lowpass filter was incorporated to block the LO leakage of the mixer.

3.3 Experimental Results for One-Dimensional Array

Figs. 3.8 and 3.9 show the normalized H-plane radiation patterns in both transmit and receive mode. Five radiation patterns are shown for each mode for a range of VCO tuning voltages. A beam-steering range of 40° is achieved, with less than 3 dB amplitude variation observed between the patterns.

The 0.97-V VCO control voltage corresponds to the 5.8-GHz LO frequency, resulting in steering at -20°. The 7.51-V VCO voltage corresponds to the 6.8-GHz LO frequency, resulting in steering at 20°.

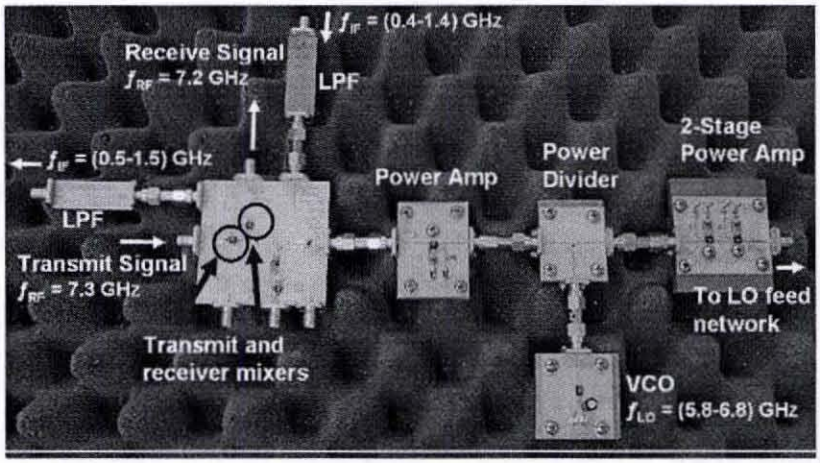

Fig. 3.7: Transmitter, receiver, and VCO circuitry.

Slight differences in the transmit and receive patterns can be attributed to differences in the feed circuitry associated with each array. The receiver and transmitter demonstrate 40° of scanning controlled by the tuning voltage of a single VCO.

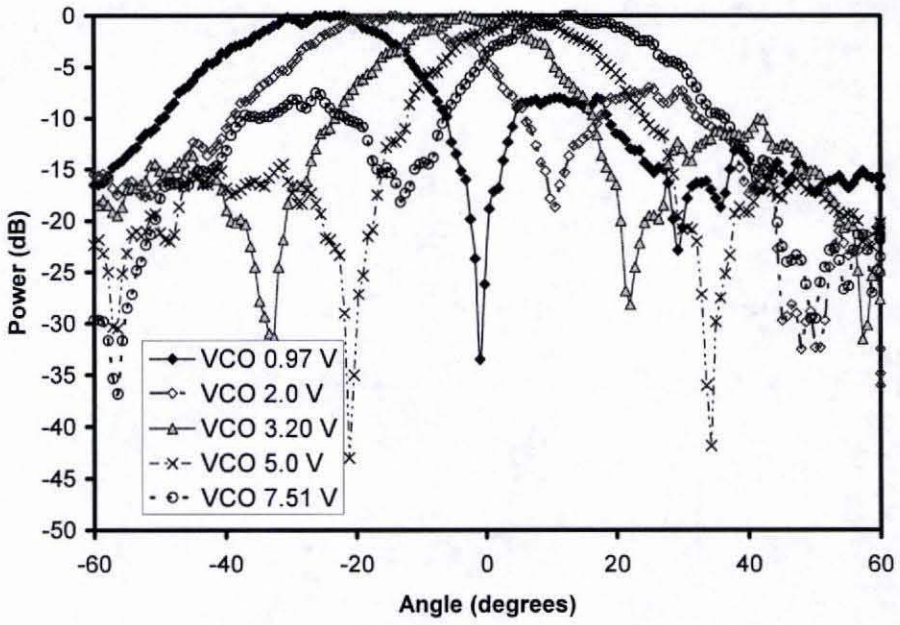

3.8: Receiver radiation patterns vs. VCO tuning voltage.

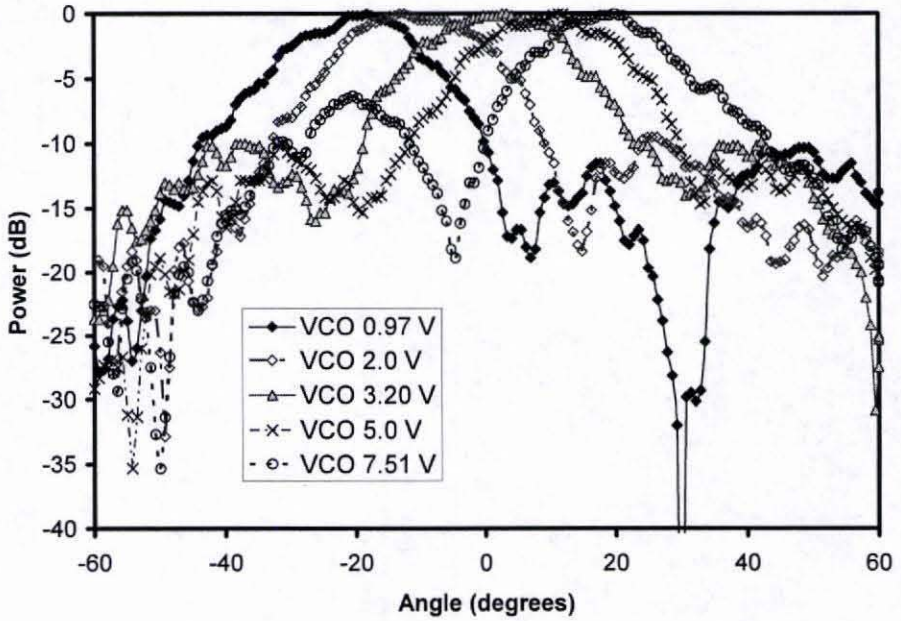

3.9: Transmit radiation patterns vs. VCO tuning voltage.

3.4 Two-Dimensional Transmit, Voltage-Controlled Phased Array

For many applications two-dimensional steering arrays are required. This section describes the first step into turning the topology of the one-dimensional full-duplex frequency-controlled phased array into two-dimensional frequency-controlled phased array by demonstrating two-dimensional transmission.

3.4.1 Two-Dimensional Beam Steering

Phase addition is used to achieve steering in the azimuth and elevation planes by mixing LO and IF signals [31]. The example in Fig. 3.10 depicts IF and LO beam-forming networks with progressive phase delays across each row and column ports. The mixer produces a signal containing the sum of the two phases. The columns contain the IF beam-forming phase progressions, while the rows contain the LO beam-forming phase progressions. Column phase progression steers the beam in the horizontal dimension, and row phase progression steers the beam in the vertical dimension.

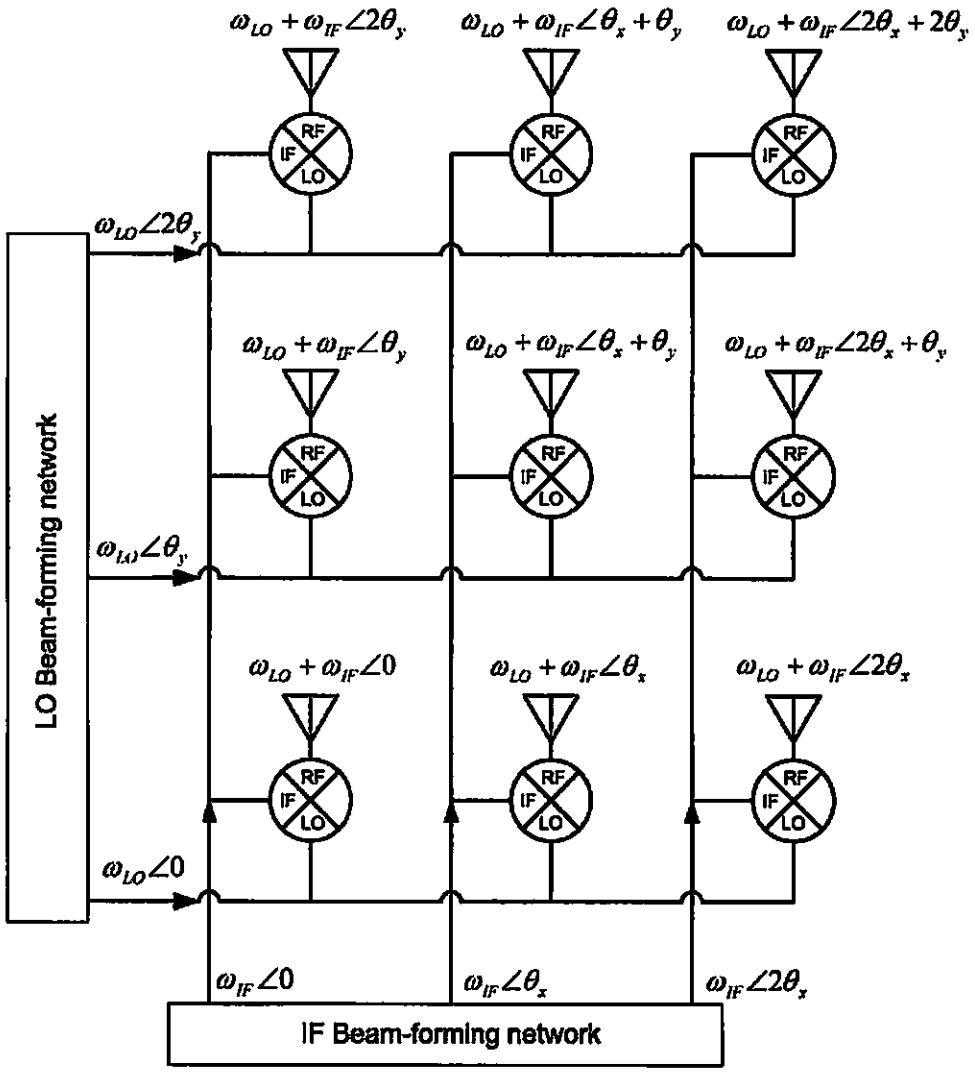

Fig. 3.10: Phase addition for achieving two-dimensional steering [31]. Column phases associated with steering in the X-dimension, row phases are associated with steering the array in the Y-dimension.

3.4.2 Design Parameters

The beam-forming networks in Fig. 3.10 are substituted with the frequency-controlled phased array networks described in Sections 3.2 and 3.3. The I/O ports for this system include the transmitted data, tuning voltages V_{DC1} and V_{DC2}, and the LO generator signal shown in Fig. 3.11.

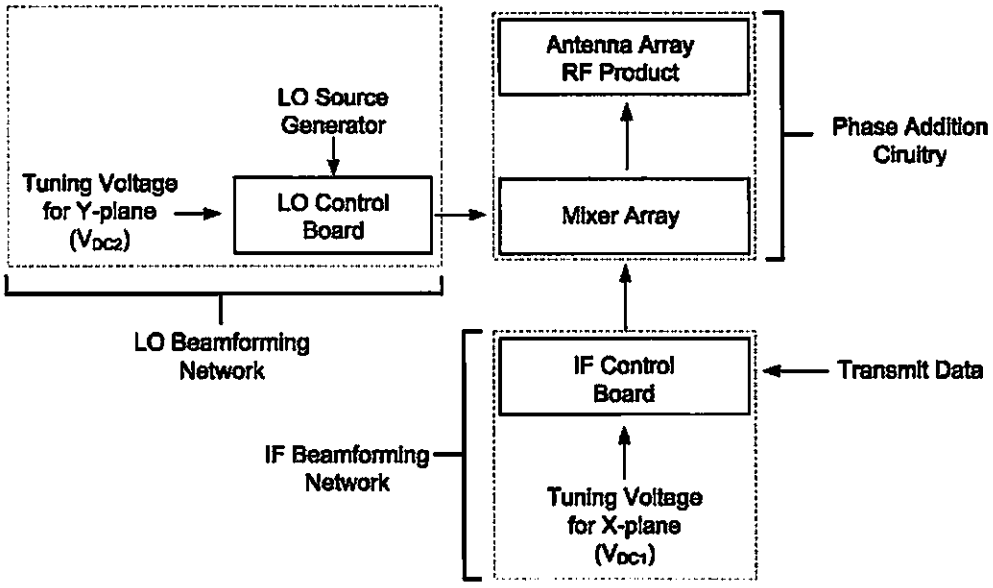

Fig. 3.11: Block diagram of two-dimensional voltage controlled array system

3.4.3 Two-Dimensional Frequency-Controlled Circuit Design

The design consists of five major components: antenna array, mixer arrays and Wilkinson power dividers, LO control board, and an IF transmit control board. The LO board controls the steering of the beam in one dimension, while the IF control board control steers the beam in the other (Fig. 3.11).

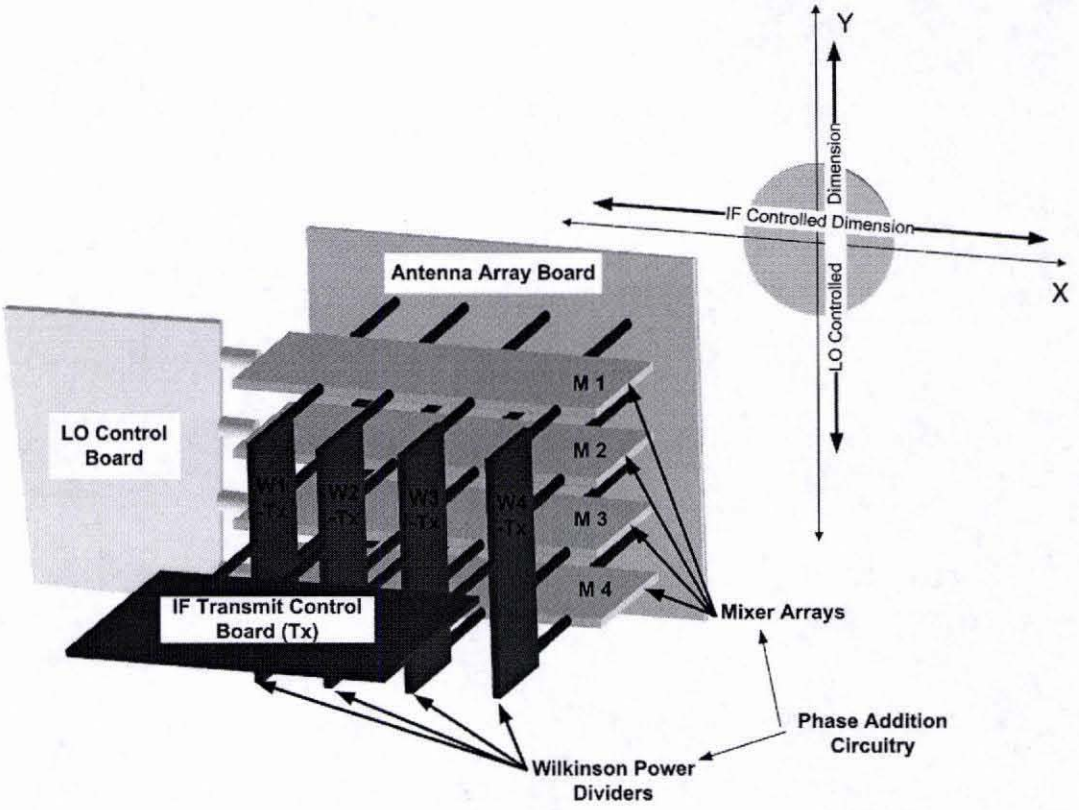

Fig. 3.12: Board level design schematic, consisting of LO and IF control boards, phase addition circuitry which includes mixer boards, Wilkenson power dividers and antenna array.

The phase addition circuitry consists of the antenna array, mixer arrays and Wilkinson power dividers. The LO control board and IF transmit control (Tx) board are the beam forming networks attached to the phase addition circuitry Fig. 3.12.

A. Antenna Array

Project members B. Takase and J. Akagi designed a 16-element array to demonstrate two-dimensional steering not only for transmission, but reception as well. The antenna design allows expansion to a full-duplex system at 6.5 GHz. Each patch is linearly polarized and excited at two separate ports (Fig. 3.13). The ports are oriented

perpendicular to one another, resulting in 30 dB isolation. One port is used in this demonstration for transmission and the other port can be used for reception.

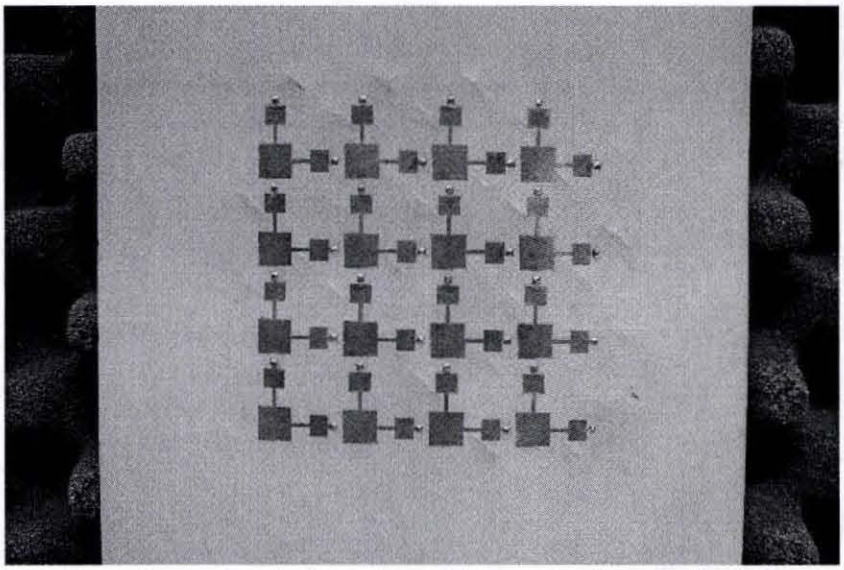

Fig. 3.13: Picture of antenna array

B. Phase Addition Mixer array and Wilkinson power dividers

The simplest implementation the phase addition circuitry consists of four mixer boards, M1 through M4, each consisting of four mixers. Each mixer is associated with one patch antenna (Fig. 3.14). Individual mixers in each row is fed in phase by the LO control board. A branchline coupler distributes power equally and the phase at each port is designed to be periodic for the LO frequency, shown in Fig. 3.14.

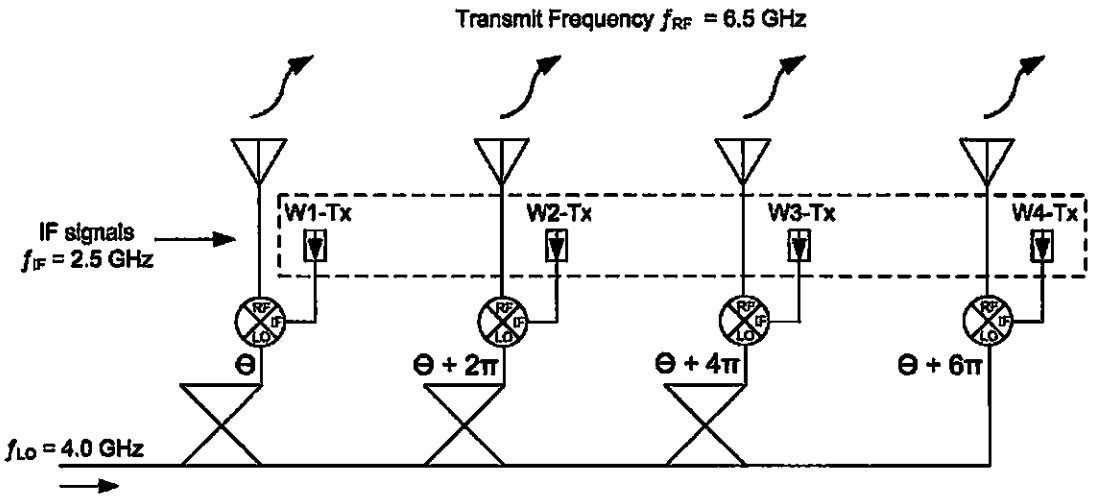

Fig. 3.14: Schematic of mixer board array, identical for boards M1 through M4 in Fig. 3.12 and Fig. 3.15.

Fig. 3.14 depicts the schematic for an individual board. To complete the phase addition circuitry, individual mixers in any given column are fed in phase by the same IF signal. As shown in Fig. 3.12, the mixer boards M1 through M4 are stacked horizontally forming rows. Vertically oriented Wilkinson power dividers (Fig. 3.12 and Fig. 3.15, W1-Tx through W4-Tx) feed the transmit mixers a 2.5-GHz signal at the IF ports in columns.

The mixers combine the LO signal f_{LO} = 4.0 GHz with the IF signal f_{IF} = 2.5 GHz. The mixed product is transmitted at f_{RF} = 6.5 GHz. Fig. 3.15 substitutes the phase addition circuitry in the block diagram (Fig. 3.12) and depicts the 16 mixers required for transmission.

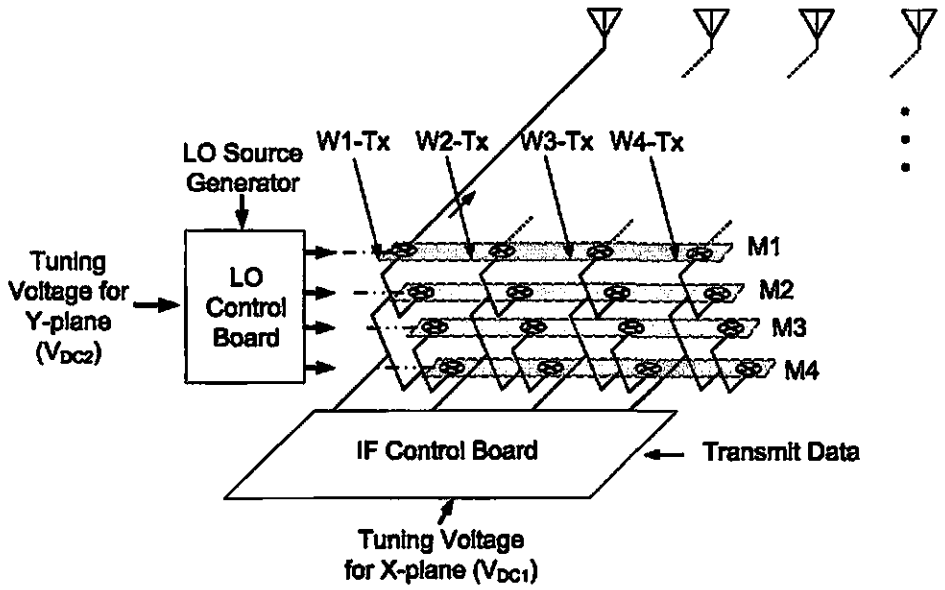

Fig. 3.15: Phase addition schematic substituted into block diagram of Fig. 3.11

C. *IF transmit control board*

The transmit control board controls the steering of the beam in the horizontal dimension. The branchline coupler, mixers, and VCOs used in the one-dimensional array are used in the transmit IF control board. As the VCO frequency changes, the phase progression at each element changes accordingly, achieving beam steering.

For demonstration purposes the transmit frequency is selected at f_{IF} = 2.5 GHz. The signal is mixed with the VCO signal f_{VCO} = (5.8-6.8) GHz and produces f_{RF} = (8.3-9.3) GHz. The f_{RF} signal is mixed with the f_{VCO} producing a f_{IF} = 2.5 GHz (Fig. 3.16).

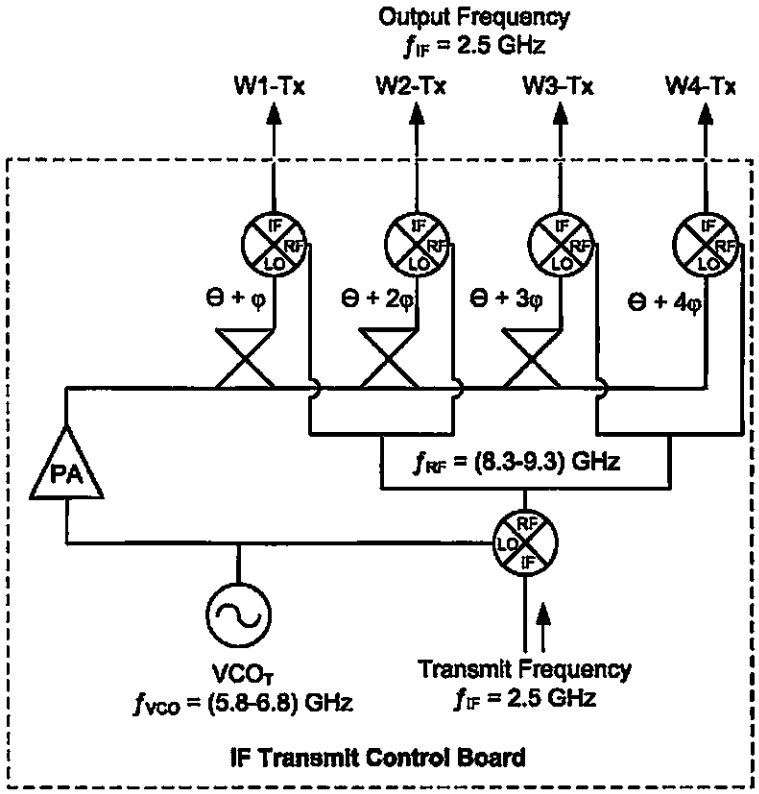

Fig. 3.16: Schematic of IF transmit control board.

D. LO control board

The LO control board uses the same topology as the IF transmit control board. The differences are signal frequencies and the amplifiers at the output stage. To avoid variances in the output power of the radiated signal, the mixers in the mixer array boards (M1 through M4) must operate in the saturated region. The LO control board is fed with a 4.0-GHz external signal source. The external source determines the output frequency of the LO board array.

Like the other control boards, the branchline coupler provides the phase delay to obtain the correct phase progression. From Fig. 3.17, the same model VCO used in the

IF boards is used in the LO board. VCO_{LO} produces f_{VCO} = (5.8-6.8) GHz and is mixed with the f_{LO_G} = 4.0 GHz signal producing a f_{RF} = (9.8-10.8) GHz. The f_{RF} and the f_{LO_G} are mixed, resulting in an IF product with a constant 4.0 GHz. The f_{LO} = 4.0 GHz (Fig. 3.17) generated differs from the f_{LO_G} = 4.0 GHz external signal by carrying the phase progression used as the LO control source for the mixer arrays M1 through M4.

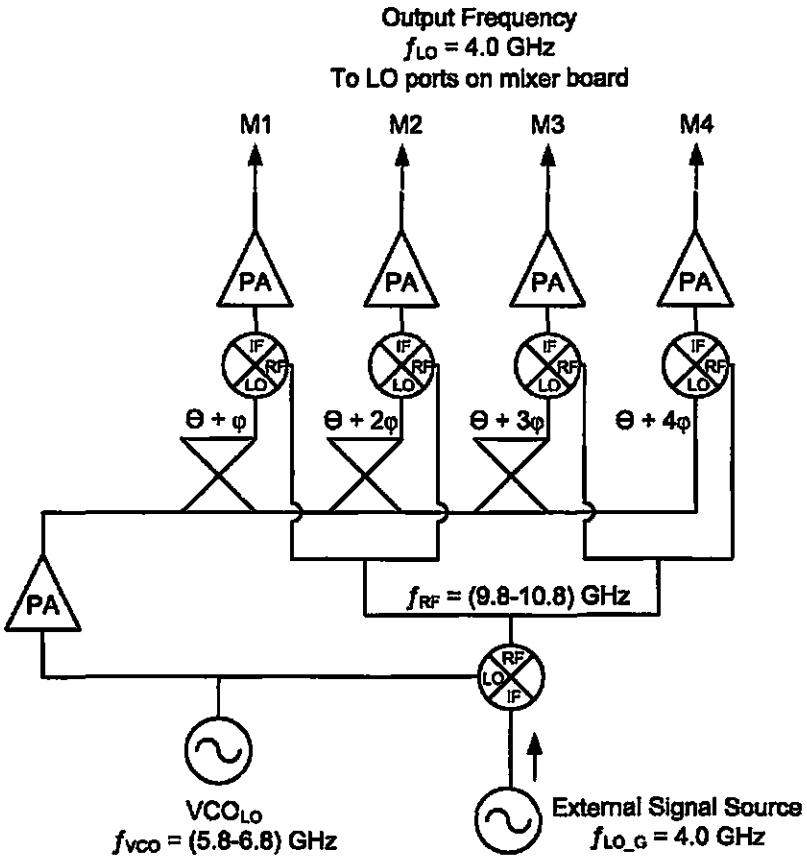

Fig. 3.17: Schematic of LO control board

3.4 Experimental Results for Two-Dimensional Array

The radiation patterns demonstrate the steering capabilities of the system. Steering in x-dimension and y-dimension are tested separately. The IF steering control in the x-dimension is tested first, the LO control board must be calibrated. 3.0 V is applied to the tuning voltage of the VCO, keeping the beam in the y-dimension at broadside. The control voltage is swept from 1.0 V to 7.0 V. Steering in the x-dimension is shown in Fig. 3.18. A steering range of 40° is demonstrated.

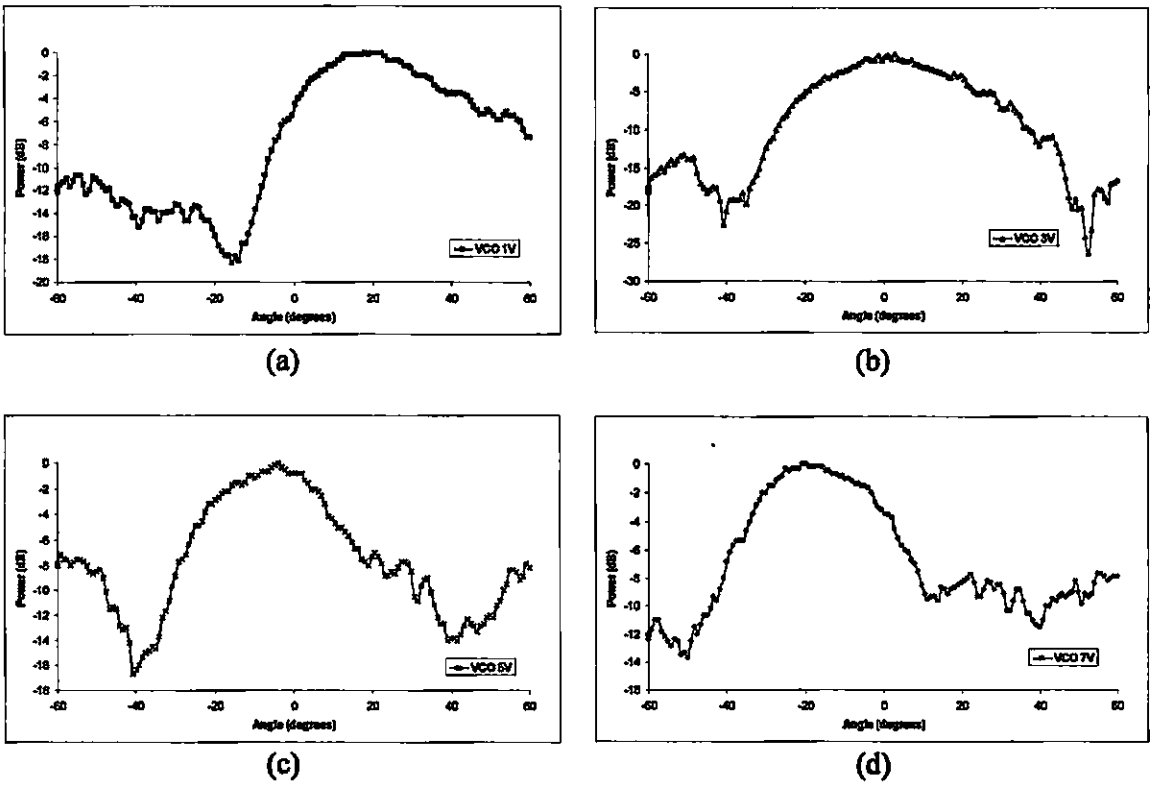

Fig. 3.18: Transmit RCS patterns demonstrating steering in x-dimension, (a) VCO control set to 1V, center at 20°, (b) VCO control set to 3V, center at 5°, (c) VCO control set to 5V center at -5°, (d) VCO control set to 7V, center at -20°.

Steering in the y-dimension requires the IF transmit board set the x-dimension beam at broadside. The VCO tuning voltage of the IF board is set to 3.0 V. The LO board VCO can be tuned from 1.0 V to 7.0 V. Fig. 3.19 demonstrates the steering capabilities of the frequency-controlled array in the y-dimension. The RCS patterns have enlarged side lobe amplitudes compared to the IF control steering in Fig. 3.18. The branchline couplers in the control boards are very sensitive to fabrication errors and are manifested in the RCS patterns. The VCO tuning voltage is set at 7 V, the main lobe is located at -15°. At 1 V the main beam is directed at approximately 25° demonstrating a steering range of 40° in the y-dimension.

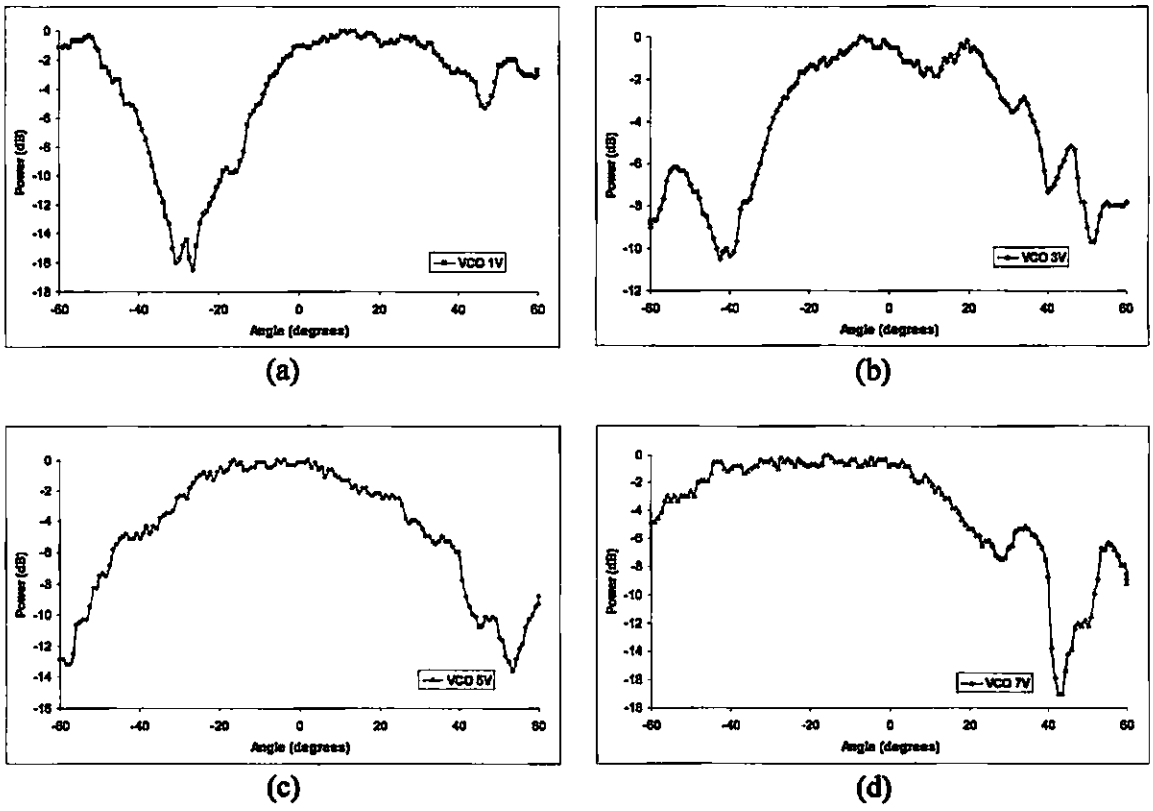

Fig. 3.19: Transmit RCS patterns demonstrating steering in y-dimension, (a) VCO control set to 1V, center at 20°, (b) VCO control set to 3V, center at 5°, (c) VCO control set to 5V center at -5°, (d) VCO control set to 7V, center at -20°.

A full-duplex frequency controlled array has been demonstrated in Section 3.2. The frequency-controlled method has also been demonstrated in a two-dimensional transmit array. The two-dimensional transmit array is expandable to a full-duplex array and discussed in Section 5.2*A*. The simple steering control of the frequency-controlled array allows for easy system integration with control hardware. Possible integration of self-steering control which is based on phase detection and power detection are discussed in Section 5.2*B* and 5.2*C* respectively.

CHAPTER 4

CHARACTERIZATION OF RECONFIGURABLE AMPLIFIER NETWORKS

4.1 Introduction

Microwave applications of micro-electromechanical systems (MEMS) technology have been steadily increasing. MEMS switches have been implemented into tunable matching networks and provide many impedance-matching configurations [32], [33]. In recent years MEMS switches have proven themselves in variable-frequency power amplifier designs [15].

The matching network configuration used to match devices such as amplifiers, mixers, etc. is shown in Fig. 4.1.

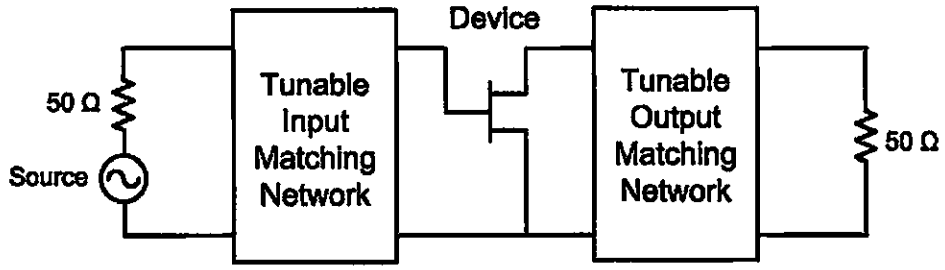

Fig. 4.1: Schematic of unknown device with input and output matching networks

Fabrication errors, fabrication discrepancies, and lifetime performance degradation becomes a concern when using a large number of MEMS switches in a network. Once MEMS switch networks are implemented in the circuit, characterization of the circuit becomes difficult. In most circuits removal of the matching network is not possible. The output measurements of the amplifier circuit determine whether the circuit

is properly functioning. If there are problems with the tunable matching network, the switches are reconfigured to compensate for individual faulty switches.

In collaboration with Northrop Grumman Space Technology (NGST), UH conducted a study of autonomous reconfigurable amplifiers and characterization of the matching networks for self-diagnosis. Fellow project member K. Ching initiated characterization of TITL networks by using transmission–line capacitive loading techniques. This chapter continues the work of [34] and introduces a method of characterizing MEMS switches implemented in a tunable amplifier configuration.

Capacitive Loading and MEMS Switches

MEMS switches have a capacitance associated with the on and off states of the switch (Fig. 4.2). The capacitance associated with a MEMS switch in the on and off states are [35]:

$$C_{on} = \frac{\varepsilon_{dielectric}\varepsilon_0 A}{h_{dielectric}} \tag{3.1}$$

$$C_{off} = \frac{1}{\frac{h_{dielectric}}{\varepsilon_{dielectric}\varepsilon_0 A} + \frac{h_{air}}{\varepsilon_0 A}} \tag{3.2}$$

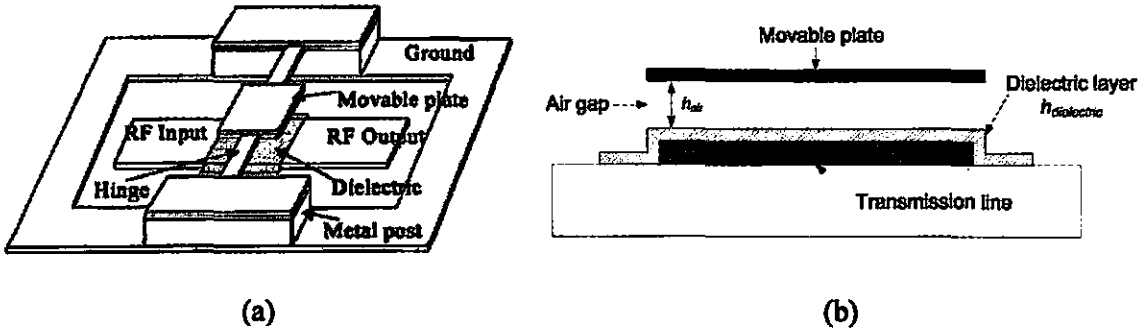

Fig. 4.2: (a) Top view of basic MEMS switch, (b) Cross-section of basic capacitive MEMS switch [5].

The capacitance of the switches is used to change the impedance of transmission lines. The simplest method of capacitively loading a transmission line is to use periodic capacitors changing the characteristic impedance and the phase velocity of the line [36]:

$$Z_0 = \sqrt{\frac{L}{C}} \text{ and } v_{phase} = \frac{1}{\sqrt{LC}} \tag{4.3}$$

NGST decided to use a 30 MEMS switch matching network design called a "tunable impedance transmission line" (TITL), shown in Fig. 4.3. Since the TITL contains 30 switches, there are 2^{30} combinations for the overall capacitance (C_{eq}) of the tuned transmission line.

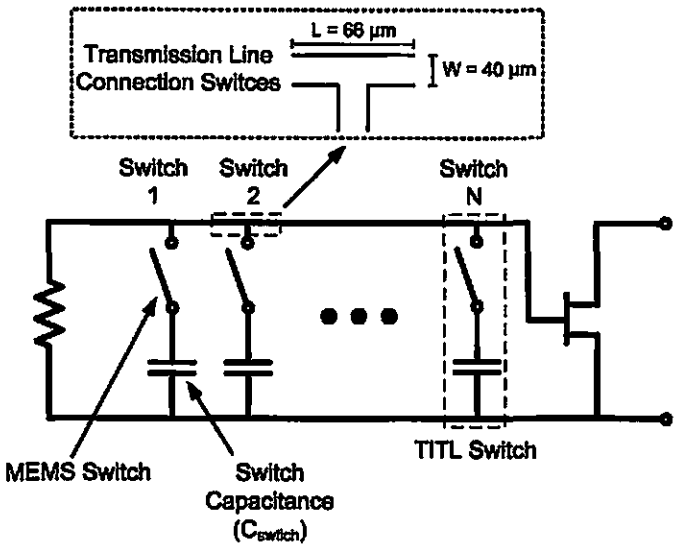

Fig. 4.3: Schematic of TITL network in input matching network configuration.

MEMS switches have a limited lifetime. Switch performance degrades over time and usage because of electromechanical characteristics [37]. Performance degradation changes the characteristic impedance of the transmission line. The initial step to compensate for failing or bad performing switches is to characterize and pinpoint the problem.

4.2 TITL Characterization Theory

The first step in characterization is to look at an individual MEMS switch. The simplest way of characterizing circuits in the shunt configuration along a transmission line is to use the ABCD parameters of lumped elements (Fig. 4.4).

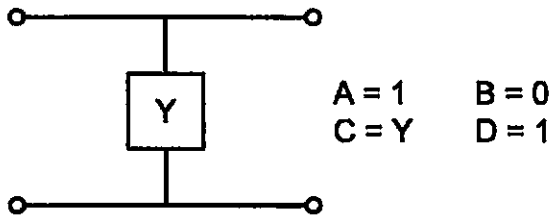

Fig. 4.4: Shunt element with associated ABCD parameters [37]

To simplify evaluation, an individual MEMS switch can be modeled as shown in Fig. 4.5. When the switch is on, the capacitance is modeled as C_{switch}. When the switch is turned off, the circuit becomes an open circuit.

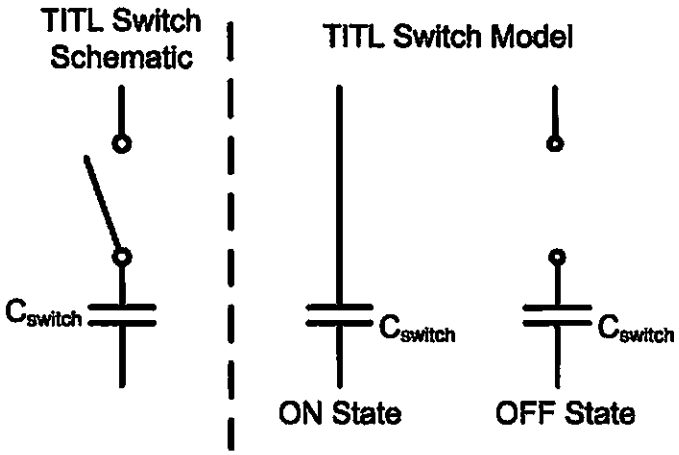

Fig. 4.5: Model of individual MEMS switch.

Using the TITL switch model the ABCD parameters for a capacitor, an open circuit stub, and transmission line are listed on Table. 4.1. The ABCD parameters are used to calculate the S parameters of entire TITL.

	ON State (Transmission Line)		OFF State (Open Circuit Stub)		Transmission Line	
ABCD Parameters	A = 1	B = 0	A = 1	B = 0	A = cos(βl)	B = j*Z_0*sin(βl)
	C = j*ω*C_{switch}	D = 1	C = 0	D = 1	C = j*Y_0*sin(βl)	D = cos(βl)

Table 4.1: ABCD parameters of switch states

To find the overall ABCD parameters, the individual ABCD parameter matrices are multiplied. The resulting ABCD matrix is converted to scattering parameters (S parameters), Fig. 4.6. The resulting S parameters of the TITL is a function of the capacitance of the switch, $S_T = S(C_{switch})$[4].

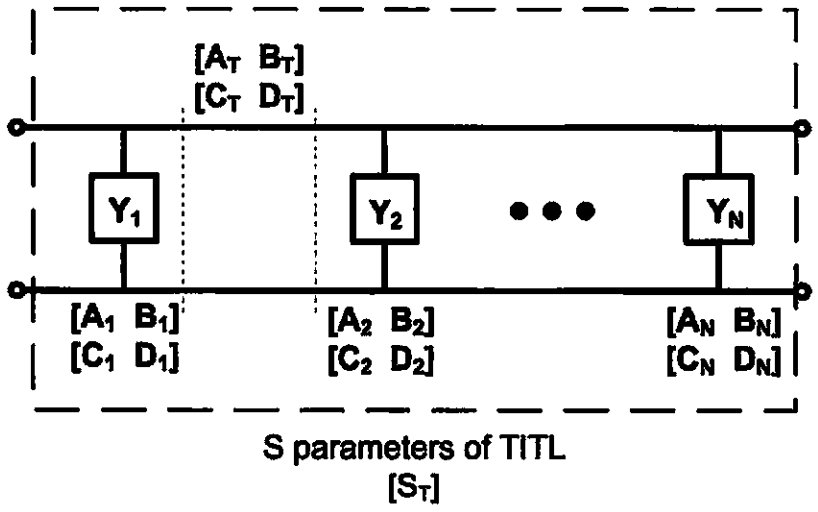

Fig. 4.6: S parameters of entire TITL

Analysis of the entire circuit, TITL, and device is required to characterize the switches. Using signal flow graph decomposition and Mason's rule, the gain of the

[4] The notation $S_T = S(C_{switch})$ represents a function $y = f(x)$, where the S parameters of the TITL, S_T is a function of the switch capacitance, C_{switch}.

amplifier circuit can be determined from the S parameters of the TITL and device (Fig. 4.7).

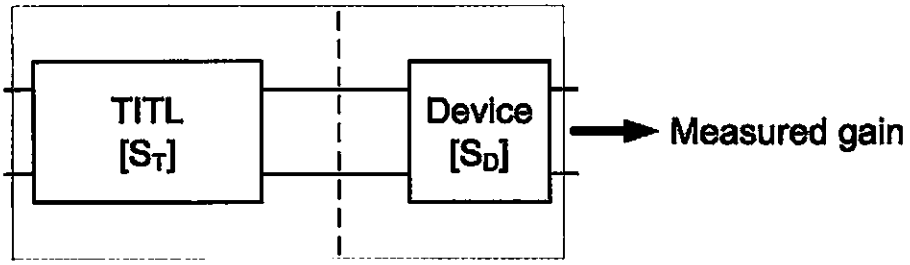

Fig. 4.7: Schematic of circuit S parameters, S_T – S parameters of the TITL, S_D – S parameters of the device

Using Mason's rule, the gain of the circuit is

$$Gain = \frac{S_{21T}S_{21D}}{1-(S_{22T}S_{11D})} \tag{4.4}$$

There are four unknowns, $S21_D$ and $S11_D$ of the device and the $S21_T$ and $S11_T$ of the TITL. $S21_T$ and $S11_T$ are symbolically expanded in terms of C_{switch} and substituted back into (4.4) resulting in

$$Gain = \frac{S(C_{switch})_{21T} \cdot S_{21D}}{1-(S(C_{switch})_{22T}S_{11D})} \tag{4.5}$$

Substituting the TITL S parameters in terms of C_{switch}, the gain equation now consists of three unknowns, C_{switch}, $S21_D$ and $S11_D$.

4.3 Symbolic Analysis

To solve for each variable, each of the three gain equations must contain all the variables. The simplest method of obtaining the three different equations is reconfiguring two switches in the TITL. Simplifying the 30 switch TITL, the first two switches are

manipulated while the other 28 are turned to the OFF state (Fig. 4.8). Table 4.2 shows the four possible combinations of two switches.

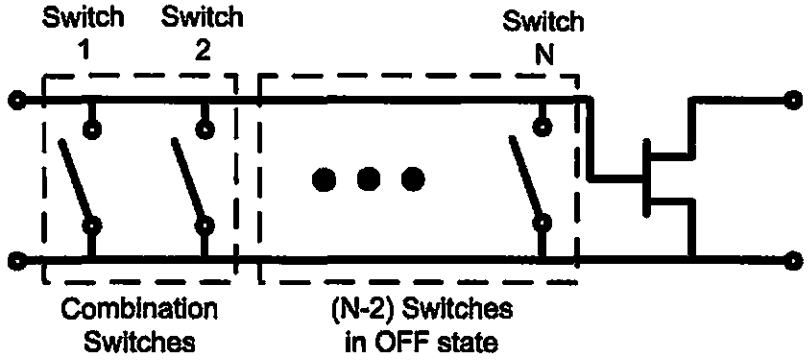

Fig. 4.8: TITL with N-switches, first two switches used in analysis, remain switches in OFF state

Switch 1	Switch 2	Resultant
ON	OFF	Gain 1
OFF	ON	Gain 2
ON	ON	Gain 3
OFF	OFF	Gain equation does not contain C_{switch}

Table 4.2: Possible combinations of two switches in the TITL

When the two switches are in the ON-OFF, OFF-ON and ON-ON states, as shown in Fig. 4.9, three unique gain equations are obtained that allow for the solution of the capacitance values. When both switches are OFF, the switches are open circuits and the TITL is a simple transmission line. The resulting gain equation does not contain the C_{switch}, so the OFF-OFF state is not used in this characterization.

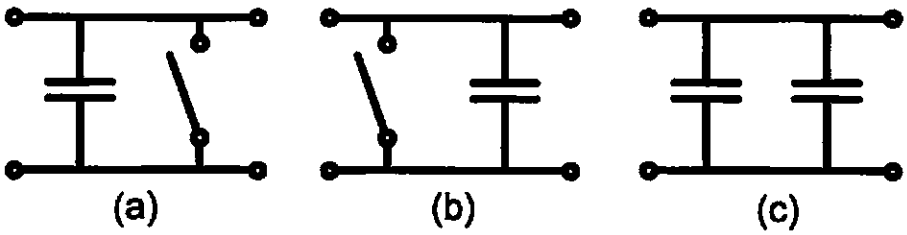

Fig. 4.9: (a) Switch 1 ON, Switch 2 OFF, (b) Switch 1 OFF, Switch 2 ON, (c) Switch 1 ON, Switch 2 ON.

MATLAB code is written to solve for the S parameters of the TITL switch. Section 1 of the MATLAB code in Appendix A uses ABCD parameters of the switch and transmission lines to find the overall ABCD parameters for each of the three different combinations of the two MEMS switches. The MATLAB code also accounts for the transmission line lengths associated with N-2 switches (Fig. 4.8). Section 2 in the MATLAB code converts the ABCD parameters of the TITL to S parameters.

Section 3 and 4 of the MATLAB program substitutes the S parameters of the three combinations of TITL networks into Mason's rule and stores the equations in memory. Using the three gain equations, algebraic substitution is used to solve for the C_{switch}.

Two equations are produced for C_{switch}. A squared C_{switch} term in the gain equation results in two solutions. Verification of this symbolic analysis is verified by microwave circuit computer simulations.

4.4 Simulation and Analysis

To verify the MATLAB code, three gain equations are taken from a microwave circuit simulator. The simulation reproduces a simple switch configuration connected to

a transistor. The three gain equations produced by the ADS simulation are inputted into the MATLAB code (Appendix A, Section 4). The MATLAB code output should result in the correct capacitance values used in the ADS simulation.

In ADS, a single Agilent 36077 transistor is connected to MEMS switches. The switches are implemented using an open circuit for the OFF configuration and a capacitor is inserted for an ON state of the switch. The capacitance value selected is 0.5 pF. To achieve the three different switch combinations in ADS, each switch combination is simulated separately. Simulation in ADS requires the additional transmission line length representing the switches N>2 (Fig. 4.10).

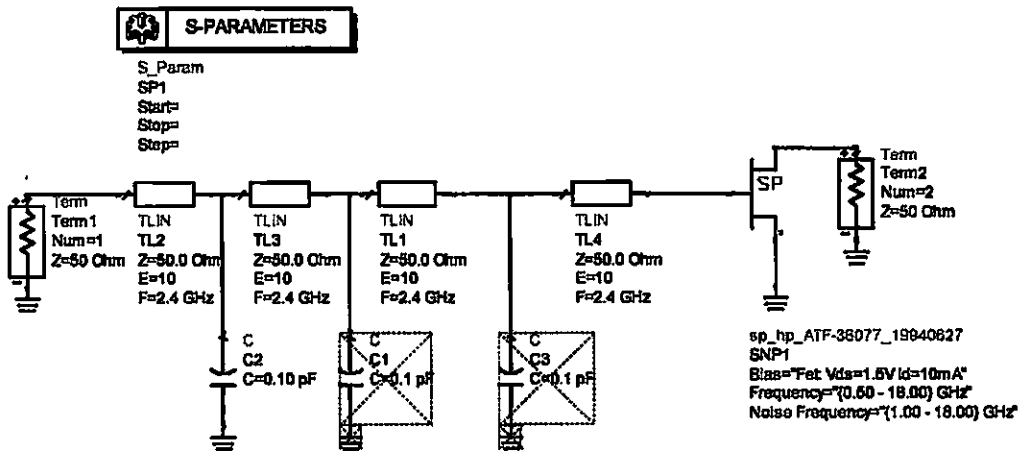

Fig. 4.10: ADS simulation schematic of TITL network connect to transistor, number of switches, N = 3.

ADS outputs the gain of the amplifier circuit. The ADS gain values and MATLAB calculated capacitance values are listed in Table 4.3.

Gains from ADS	
Gain 1 from ADS	-0.0478 + 3.4419i
Gain 2 from ADS	-0.7252 + 3.9744i
Gain 3 from ADS	-0.5218 + 4.0377i
Capacitance Values from MATLAB Code	
Capacitance 1	**5.0006e-013 -4.5799e-017i**
Capacitance 2	**5.8850e-012 +7.6682e-014i**

Table 4.3: Complex gain of amplifier circuitry from ADS simulation and capacitance values calculated by MATLAB code.

The results present two values for the capacitance. The correct capacitance value is 0.5 pF or $5.0e^{-13}$ F with no imaginary component. Observing both capacitances the MATLAB code produces, the correct value for the capacitance contains a smaller imaginary part, Capacitance 1 from Table 4.3. The MATLAB code uses rounded gain values from ADS and produced the correct capacitance value by manipulating only two switches in the N-switch TITL.

4.5 Applications

A. Determining the Value of C_{switch}

The MATLAB code in the previous section is used to characterize the TITL. Once the capacitance of the switch is known, any ON and OFF switch configurations can be analyzed and predict the expected gain of the amplifier circuitry.

By manipulating two of the switches in the TITL, the value of C_{switch} can be determined with three different overall gain measurements. The simulations were based on a system consisting of a TITL chip connected to an unknown device. The procedure

for this manipulation was described in the previous section. The MATLAB code only returned an equation for C_{switch} in terms of these three gain simulations for certain pairs of manipulated switches, but may be expanded to calculate C_{switch} for any pair of manipulated switches. Once C_{switch} is calculated for a sufficient number of switch pairs, a representative value of C_{switch} may be determined. The impedance of the TITL might then be found for any combination of ON or OFF switches.

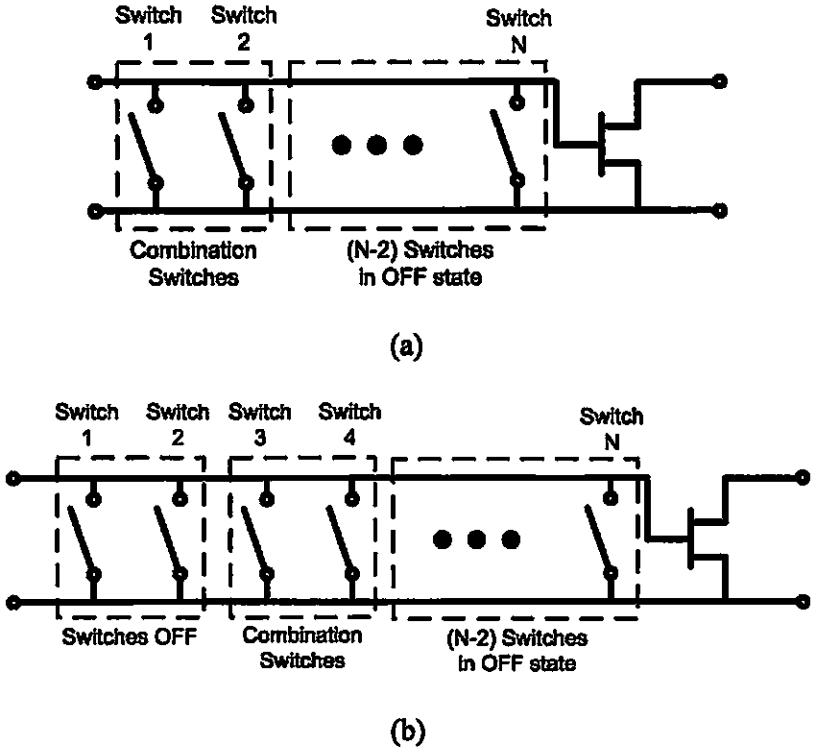

Fig. 4.11: (a) First two switches used to get 3 unique combinations. (b) First two switches are turned off; second pair of switches is used to solve for the capacitance value of switches 3 and 4.

B. Testing for Faulty Switches in the TITL

Once the value of C_{switch} is found as described above, faulty switches can be tested for while the TITL is embedded with the unknown device. A single switch can be set to the ON state while the rest of the switches are left in the OFF state.

Since the value of C_{switch}, $S21_D$, and $S11_D$ were previously solved, the gain of the entire circuit can be calculated for any configuration of the TITL. A faulty TITL switch can be detected by comparing the predicted gain value to the measured gain of the circuit.

CHAPTER 5

CONCLUSIONS AND FUTURE WORK

5.1 Conclusions

This thesis presented advances in satellite-to-satellite communication systems, mobile terrestrial to satellite systems, and a method of characterizing a class of reconfigurable circuits.

A pair of nanosatellites was presented and discussed in Chapter 2, demonstrating a 10.5-GHz two-dimensional retrodirective array for small-satellite communications. The quadruple subharmonic mixing technique achieved phase conjugation and eliminated the need for a high-frequency LO source. One satellite housed the eight-element two-dimensional array with eight circularly polarized patch antennas and communicated with a transponder satellite.

A one-dimensional and two-dimensional voltage-controlled analog phased array was described and verified in Chapter 3. Many mobile communication systems require a fast tracking highly directive communication link. Electronically steered arrays provide fast analog operation. A scanning range of 40° was demonstrated in one-dimension and a scanning range of 40° in each axis in shown in the two-dimensional prototype.

As the demand for multi-frequency communications increases so does the demand for MEMS tunable matching networks. Chapter 4 introduced a simplification of unknown MEMS switches in a TITL and a method for switch characterization. MATLAB solving code was written requiring only three gain measurements of the

amplifier module. The characterization code was verified using ADS simulation gain measurements.

5.2 Suggestions for Future Work

A. Two-dimensional Full-duplex Frequency-Controlled Phased Array

The full-duplex capabilities demonstrated in one-dimensional frequency-controlled array in Section 3.2 can be applied to the two-dimensional transmit frequency-controlled array demonstrated in Section 3.4. A receiving two-dimensional frequency-controlled array is easily integrated into the current two-dimensional transmit system by creating another set of mixer arrays and a set of mirror image LO and IF control boards (Fig. 5.1 and Fig. 5.2). Like the one-dimensional array, two sets of circuitry are implemented, one for transmission and the other for reception. The antenna array in Section 3.4.3*A* has been designed with full-duplex expansion capabilities. One polarization plane of the antenna will be dedicated for transmission and the other for reception. The control voltages for both systems are linked together, receive and transmit arrays steer simultaneously in the same direction (Fig. 5.3).

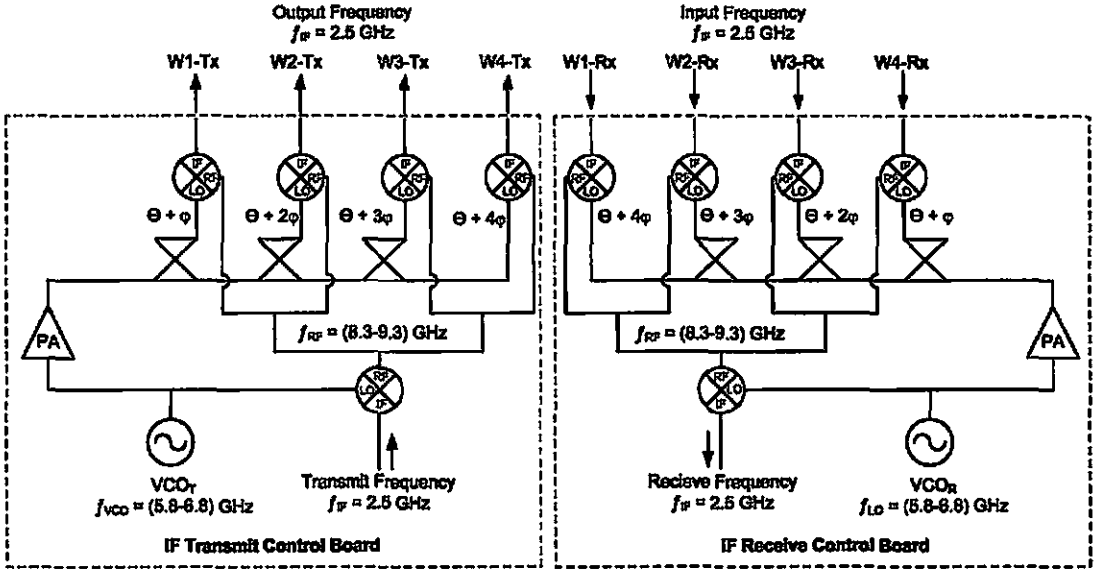

Fig. 5.1: Transmit and receive IF control boards

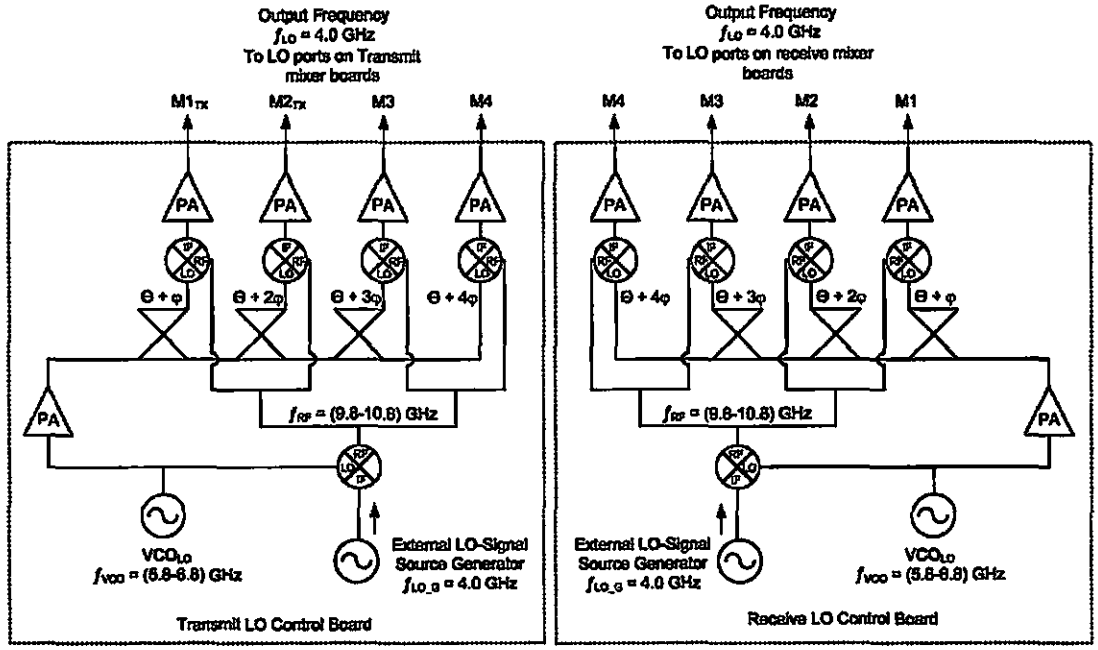

Fig. 5.2: Transmit and receive LO control boards

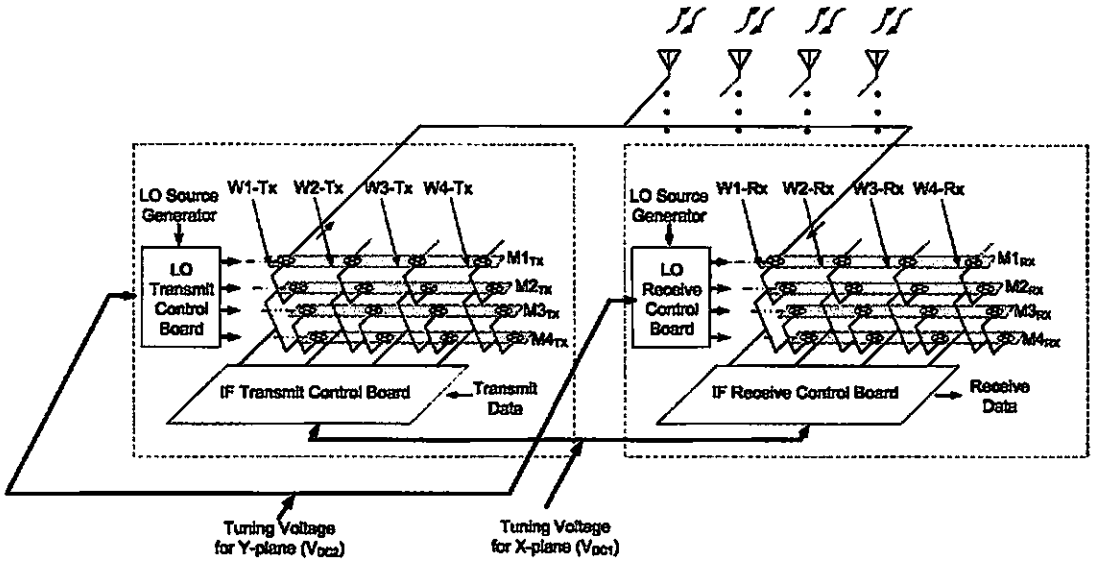

Fig. 5.3: Schematic of two-dimensional full-duplex frequency-controlled array

B. Retrodirective Frequency-Controlled Array Using Phase Detection

A full-duplex two-dimensional frequency-controlled array has been proposed in the previous section. Future work could possibly include control circuitry that would make the array self-steering. A phased controlled scheme as in [38] can be modified to work with the frequency controlled array (Fig. 5.4). The phase detector compares the phases at two elements. As the difference in phases increases across two antenna elements due to a larger θ_R, the output voltage of the detector increases. As the angle from broadside increases, the phase detector inherently increases the output voltage causing the frequency-controlled phased array to steer accordingly. If the signal is received at broadside, $\theta_R = 0°$, $V_{STEER} = 0$ V and results in $V_{CONTROL} = V_{BROADSIDE}$, steering the main beam broadside, $\theta_T = 0°$. The phase detector forms a feed back loop for the system, allowing the phased array to automatically steer the beam in the opposite direction as the received signal.

The expected difficulty of this design is the calibration of the V_{STEER} voltage. If the frequency-controlled phased array uses the same tunable VCO used in Chapter 3, the maximum steering range is 1-7 V based on the VCO tuning voltage. The amplifier A in Fig. 5.4 must be calibrated so the output voltage V_{STEER} correlates to the tuning voltage range of 1-7 V allowing $\theta_R = \theta_T$.

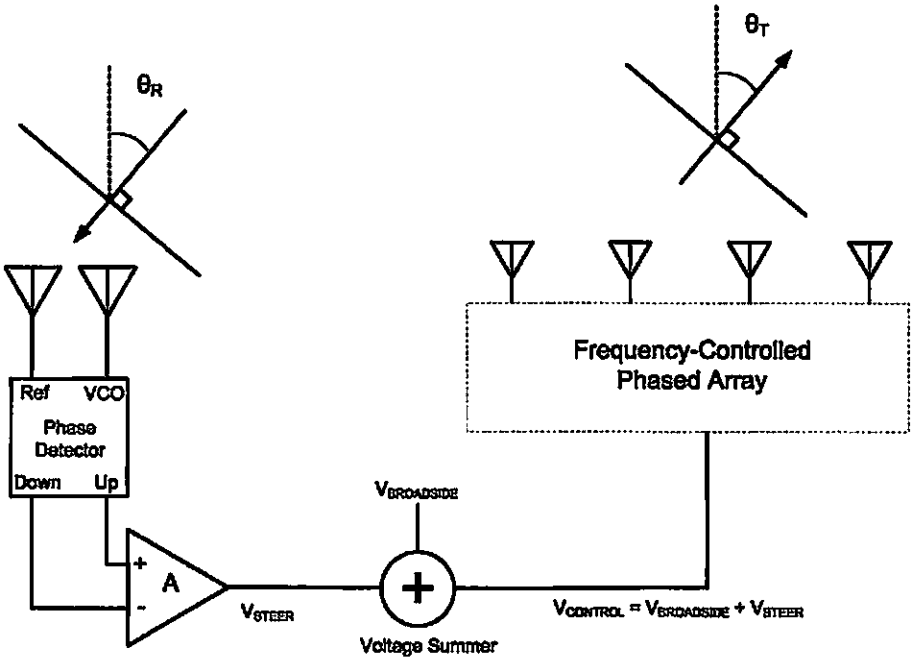

Fig. 5.4: Proposed schematic for phase detecting control circuitry for a self-steering phase detecting frequency-controlled array

C. Retrodirective Frequency-Controlled Array Using Power Detection

Another scheme based on power detection across antenna elements can be implemented as a feedback loop. A power detector converts the power received to a voltage signal. A differentiator circuit uses the voltage from the power detector and outputs a voltage signal. The differentiator outputs a positive or negative voltage dependant on the change in detected power. If the receive power increases the derivative

circuit outputs a positive voltage, if the receive power decreases the output voltage. The differentiator voltage controls the output voltage of a potentiometer. A positive differentiator voltage increases the voltage output of the potentiometer ($V_{CONTROL}$) and a negative voltage decreases the potentiometer voltage. $V_{CONTROL}$ (Fig. 5.5) increases and decreases as the power detected increases and decreases.

A major concern is the appearance of side lobes in the receive power pattern. Fig. 5.6(a) depicts the receive radiation pattern with one main lobe while Fig. 5.6(b) depicts a receive pattern with two lobes. In a typical communication system, multiple lobes are common, making it difficult to select the correct lobe to track. Selective circuitry must be added to scan the entire steering range and select the correct lobe to track.

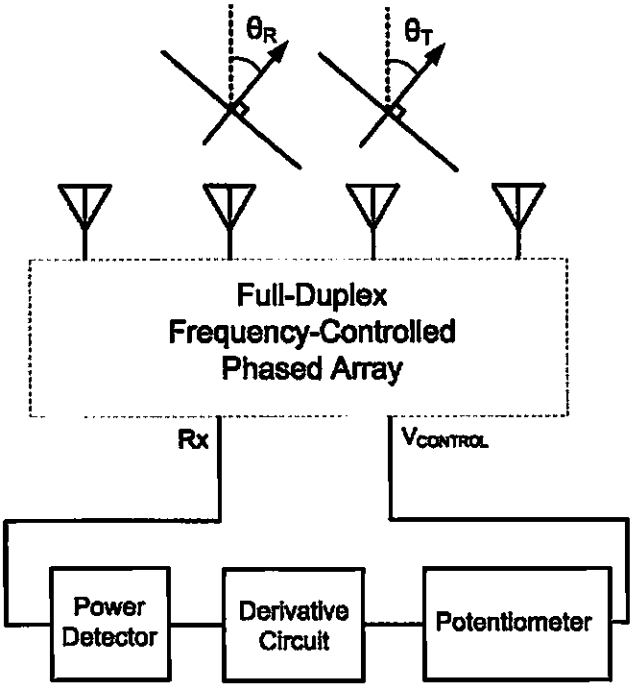

Fig. 5.5: Proposed schematic for power detecting control circuitry for a self-steering power detecting frequency-controlled array

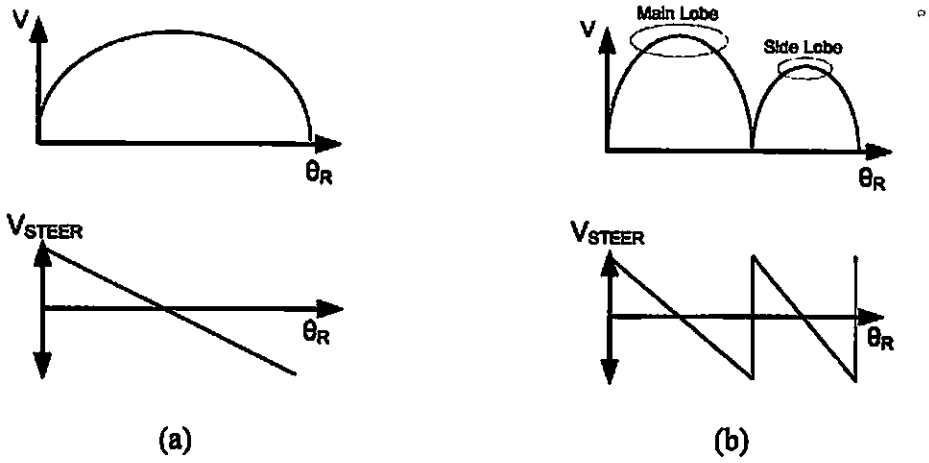

Fig. 5.6: (a) Receive power with one main lobe and V_{STEER} graph associated with receive power, (b) Receive power with main and side lobe and V_{STEER} graph associated with receive power

APPENDIX A – MATLAB Code for TITL Characterization

```
%------------------- SECTION 1 ------------------------%

%---------- TITL CHARACTERIZATION SETUP ----------%
syms Beta L w Cap S21Dev S11Dev

N = input('Please input the number of switches: ');

A = cos(Beta*L);
B = j*50*sin(Beta*L);
C = j*(1/50)*sin(Beta*L);
D = cos(Beta*L);
ABCD = [A B; C D];

%Open switch (OFF)
ABCDopen = [1 0; 0 1];

%Cap Switch (ON)
ABCDcap = [1 0; j*w*Cap 1];

%   Switch states (ON ON)     gain equation 1
TITL_ON_ON = ABCD*ABCDcap*ABCD*ABCDcap*[ABCD^((N-2)+1)];

%   Switch states (ON OFF)    gain equation 2
TITL_ON_OFF = ABCD*ABCDcap*ABCD*ABCDopen*[ABCD^((N-2)+1)];

%   Switch states (OFF ON)    gain equation 3
TITL_OFF_ON = ABCD*ABCDopen*ABCD*ABCDcap*[ABCD^((N-2)+1)];

%TITL_ON_ON gain eq 1
AT11 = TITL_ON_ON(1,1);
BT11 = TITL_ON_ON(1,2);
CT11 = TITL_ON_ON(2,1);
DT11 = TITL_ON_ON(2,2);

%TITL_ON_OFF gain eq 2
AT10 = TITL_ON_OFF(1,1);
BT10 = TITL_ON_OFF(1,2);
CT10 = TITL_ON_OFF(2,1);
DT10 = TITL_ON_OFF(2,2);

%TITL_OFF_ON gain eq 3
AT01 = TITL_OFF_ON(1,1);
BT01 = TITL_OFF_ON(1,2);
CT01 = TITL_OFF_ON(2,1);
DT01 = TITL_OFF_ON(2,2);
```

```
%------------------- SECTION 2 ------------------------%
%--------------- CONVERSION TO S PARAMETERS ------------%

%ABCD to S parameter conversion formulas taken from [37]

%TITL_ON_ON gain eq 1
S11T11=(AT11+BT11/50-CT11*50-DT11)/(AT11+BT11/50+CT11*50+DT11);
S12T11=(2*(AT11*DT11-BT11*CT11))/(AT11+BT11/50+CT11*50+DT11);
S21T11=(2/(AT11+BT11/50+CT11*50+DT11));
S22T11=(-AT11+BT11/50-CT11*50+DT11)/(AT11+BT11/50+CT11*50+DT11);

%TITL_ON_OFF gain eq 2
S11T10=(AT10+BT10/50-CT10*50-DT10)/(AT10+BT10/50+CT10*50+DT10);
S12T10=(2*(AT10*DT10-BT10*CT10))/(AT10+BT10/50+CT10*50+DT10);
S21T10=(2/(AT10+BT10/50+CT10*50+DT10));
S22T10=(-AT10+BT10/50-CT10*50+DT10)/(AT10+BT10/50+CT10*50+DT10);

%TITL_OFF_ON gain eq 3
S11T01=(AT01+BT01/50-CT01*50-DT01)/(AT01+BT01/50+CT01*50+DT01);
S12T01=(2*(AT01*DT01-BT01*CT01))/(AT01+BT01/50+CT01*50+DT01);
S21T01=(2/(AT01+BT01/50+CT01*50+DT01));
S22T01=(-AT01+BT01/50-CT01*50+DT01)/(AT01+BT01/50+CT01*50+DT01);

%------------- END OF CHARACTERIZATION SETUP -------------%


%------------------- SECTION 3 ------------------------%
%------------- BEGIN OF GAIN EVALUATION ------------------%

%gain 1 ON_ON
gain1 = (S21T11*S21Dev)/(1-(S22T11*S11Dev));

%gain 2 ON_OFF
gain2equation = (S21T10*S21Dev)/(1-(S22T10*S11Dev));

%gain 3 OFF_ON
gain3equation = (S21T01*S21Dev)/(1-(S22T01*S11Dev));

%------------- ALGERBRAIC SUBSTITUTION ------------------%

temp = char(gain1);
temp2 = strcat('gain1=',temp);
tempS21Dev = solve(temp2,'S21Dev');
%S21Dev = in terms of S11Dev, Cap, Gain

%Entering S21Dev into gain2 equation, solving for S11Dev
gain2 = subs(gain2equation, S21Dev, tempS21Dev);

temp = char(gain2);
temp2 = strcat('gain2=',temp);
```

```
tempS11Dev = solve(temp2, 'S11Dev');

%Using gain3, substituting S21Dev and S11Dev, solving for cap
tempgain3 = subs(gain3equation, S21Dev, tempS21Dev);
gain3 = subs(tempgain3, S11Dev, tempS11Dev);

temp = char(gain3);
temp2 = strcat('gain3=',temp);

%Solving for capacitance
tempCap = solve(temp2, 'Cap');

%Displaying capacitance values (two values equation contains sqrt)
capacitance1 = (tempCap(1,1));
capacitance2 = (tempCap(2,1));

%--------------- END OF SYMBOLIC ANALYSIS -------------%


%------------------- SECTION 4 ------------------------%
%--------------- START NUMERICAL ANALYSIS -------------%

%INPUT FROM USER
freq = input('\nPlease enter frequency (Hz):');
wavelength = (3*10^8)/(freq);
eleclength = input('\nPlease enter electrical length of transmission
lines (degrees): ');
%END OF INPUT FROM USER

%2*pi/(wavelength)
Beta = (2*pi)/wavelength;

%Lengths of the transmission line (10 electrical degrees)
L = (eleclength*pi/180)/Beta;

%2*pi*(frequency)-----> 2.4 GHz
w=2*pi*freq;

%Assuming Capacitance = 0.5 pF  EXAMPLE VALUE
%Cap = .5*10^-12;

syms gain1 gain2 gain3

%INPUT FROM USER
gain1 = input('\nEnter gain1 switch config ON_ON: ');
%gain1 =  -0.0478 + 3.4419*i;    % example taken from ADS

gain2 = input('\nEnter gain2 switch config ON_OFF: ');
%gain2 =  -0.7252 + 3.9744*i;    %example from ADS

gain3 = input('\nEnter gain3 switch config OFF_ON: ');
%gain3 =  -0.5218 + 4.0377*i;    %example from ADS
%END OF INPUT FROM USER
```

```
%Displaying numerical value of capacitance
cap1 = subs(capacitance1)
cap2 = subs(capacitance2)

%--------------- END OF NUMERICAL ANALYSIS -------------%
```

REFERENCES

[1] "Sea Launch to Launch Two Spaceway Satellites." Retrieved July 03, 2006 from, www.spaceandtech.com.

[2] "Satellite seeks broadband re-entry." Retrieved July 03, 2006 from, news.com.com.

[3] "SPACEWAY™ North America." Retrieved July 03, 2006 from, www.boeing.com.

[4] HONOLULU ADVERTISER, 2005. Marine's ability to communicate on the run gets a boost. *Honolulu Advertiser*, 9 Sep. 2005.

[5] M. Skolnik, *Introduction to Radar Systems, Second Edition*. New York: McGraw-Hill Book Company, 1980.

[6] E. Pels and W. Liang, "A method of array steering by means of phased control through heterodyning," *IRE Trans. Antennas Propagat.*, vol. AP-10, p. 100, Jan. 1962.

[7] M. Kim, J. B. Hacker, A. L. Sailer, and J. H. Hong, "A heterodyne-scan phased array antenna," *IEEE Microwave and Guided Wave Letters*, vol. 9, pp. 535 537, Dec. 1999.

[8] T. Nishio, H. Xin, Y. Wang, and T. Itoh, "A frequency-controlled active phased array," *IEEE Microwave and Wireless Comp. Letters*, vol. 14, pp. 115-117, Mar. 2004.

[9] T. Nishio, Y. Wang, and T. Itoh, "A novel K-band frequency-controlled beam-steering quasi-Yagi array with mixing frequency compensation," 2002 *IEEE MTT-S Int. Microwave Symp. Dig.*, pp. 1345-1348, Jun. 2002.

[10] T. Nishio, Y. Wang, and T. Itoh, "A frequency-controlled beam-steering array with mixing frequency compensation for multichannel applications," *IEEE Trans. Antennas Propagat.*, vol. 52, pp. 1039-1048, Apr. 2004.

[11] J. D. Kraus, *Antennas*. New York: McGraw-Hill, Inc., 1988.

[12] L. C. Van Atta, Electromagnetic Reflector. U.S. Patent #2,908,002, Oct. 6, 1959.

[13] C.Y Pon, "Retrodirective Array using the Heterodyne Technique," *IEEE Trans. Antennas Propagat.*, vol. AP-12, pp 176-180, Dec. 1964.

[14] "Small-Satellite Costs." Retrieved July 03, 2006 from, www.aero.org.

[15] Y. Lu, D. Peroulis, S. Mohammadi, L.P.B.Katehi, "A MEMS Reconfigurable Matching Network for a Class AB Amplifier," *IEEE Microwave and Wireless Components Letters*, vol. 13. No. 10, Oct. 2003.

[16] B. Murakami, J. Roque, S. Sung, G. Shiroma, R. Miyamoto, W. Shiroma, "A quadruple subharmonic phase-conjugating array for secure picosatellite crosslinks," *IEEE MTT-S International Microwave Symposium*, vol. 3, pp 1687- 1690, June 2004.

[17] J. Roque, B. Murakami, S. Sung, G. Shiroma, R. Miyamoto, and W. Shiroma, "Progress in Self-Steering Antennas for Small-Satellite Networks," *Space 2004 Conference*, San Diego, CA, Sep. 2004.

[18] J. Roque, S. Sung, B. Murakami, G. Shiroma, R Miyamoto, W. Shiroma, "A coupled-antenna interrogator/receiver for retrodirective crosslinks in a distributed nanosatellite network," *IEEE/ACES International Conference on Wireless Communications and Applied Computational Electromagnetics*, Honolulu, HI, pp 610-613, Apr. 2005.

[19] University Nanosat Program Website, www.university nanosat.org.

[20] AFRL Internal Cargo Unit User's Guide, 2004.

[21] AFRL Configuration Management Guide, 2004.

[22] B. T. Murakami, M. A. Tamamoto, A. T. Ohta, G. S. Shiroma, R. Y. Miyamoto and W. A. Shiroma, "Self-steering antenna arrays for distributed picosatellite networks," *in Proc. of the 17th Annual AIAA/USU Conference on Small Satellites*, Logan, UT, Aug. 2003.

[23] S. Maas, *Nonlinear Microwave and RF Circuits, Second Edition.* Boston: Artech House, 1997.

[24] G. Shiroma, 2004. *Self-Steering Arrays for Wireless Communication Networks.* Thesis (M.S.). University of Hawaii.

[25] T. Brabetz, V. F. Fusco, and S. Karode, "Balanced subharmonic mixers for retrodirective-array applications," *IEEE Trans. Microwave Theory Tech.*, vol. 49, pp. 465-469, Mar. 2001.

[26] J. Y. Park, K. M. Leong, G. R. Kim, J. I . Choi, and T. Itoh, "Active retrodirective array with subharmonic phase conjugation mixers," *in Proc. Of the 2003 Asia-Pacific Microwave Conference*, Seoul, Korea, Nov. 2003.

[27] C. Balanis, *Antenna Theory Analysis and Design, Second Edition.* New York: John Wiley & Sons, Inc., 1997.

[28] W. Stutzman, G. Thiele, *Antenna Theory and Design.* New York: John Wiley & Sons, Inc., 1998.

[29] J. Roque, G. Shiroma, W. Shiroma, "A Full-Duplex, Single-Frequency-Controlled Phased Array," *IEEE MTT-S Int. Microwave Symp,* San Francisco, CA, Jun 2006.

[30] K. Aamo, "Frequency controlled antenna beam steering," 1994 *IEEE MTT-S Int. Microwave Symp. Dig.*, pp. 1549 1552, Jun.1994.

[31] Friis, H. T., Feldman, C. B. (1937). Multiple Unit Steerable Antenna. Proc. IRE 25, 841-917.

[32] T. Vaha-Heikkila, J. Varis, J. Tuovinen, G. M. Rebeiz, "A 20-50 GHz RF MEMS single-stub impedance tuner," *in Microwave and Wireless Components Letters*, vol. 15, Issue 4, pp 205-207, Apr. 2005.

[33] J. Papapolymerou, K. L. Lange, C. L. Goldsmith, A. Malczewski, J. Kleber, "Reconfigurable Double-Stub Tuners Using MEMS Switches for Intelligent RF Front-Ends," *IEEE Transactions On Microwave Theory and Techniques*, vol. 15, No. 1, Jan. 2003.

[34] K. Ching, 2005. *Novel Reconfigurable Amplifier Design Techniques.* Thesis (M.S.). University of Hawaii

[35] J. Y. Park, G. H. Kim, K. W. Chung, J. U. Bu, "Electroplated rf MEMS capacitive switches," *Micro Electro Mechanical Systems*, Miyasaki, Japan, pp 639-644, Jan. 2000.

[36] D. Pozar, *Microwave Engineering, Second Edition.* New York: John Wiley & Sons, Inc., 1998.

[37] D. Becher, R. Chan, M. Hattendorf, M. Feng, "Reliability Study of Low-Voltage RF MEMS Switches," *GaAs MANTECH Conference*, San Diego, CA, Mar. 2002.

[38] G. Shiroma, R. Miyamoto, W. Shiroma, "A Full-Duplex Dual-Frequency Self-Steering Array Using Phase Detection and Phase Shifting," *IEEE Transaction on Microwave Theory and Techniques*, vol. 54, No. 1, Jan 2006